AD-A048 362 AIR FORCE INST OF TECH WRIGHT-PATTERSON AFB OHIO SCH--ETC F/G 20/6
LASER AUTOREFLECTANCE.(U)
DEC 77 C W MARTIN
UNCLASSIFIED AFIT/GEP/PH/77D-7 NL

1 OF 2
AD
A048 362

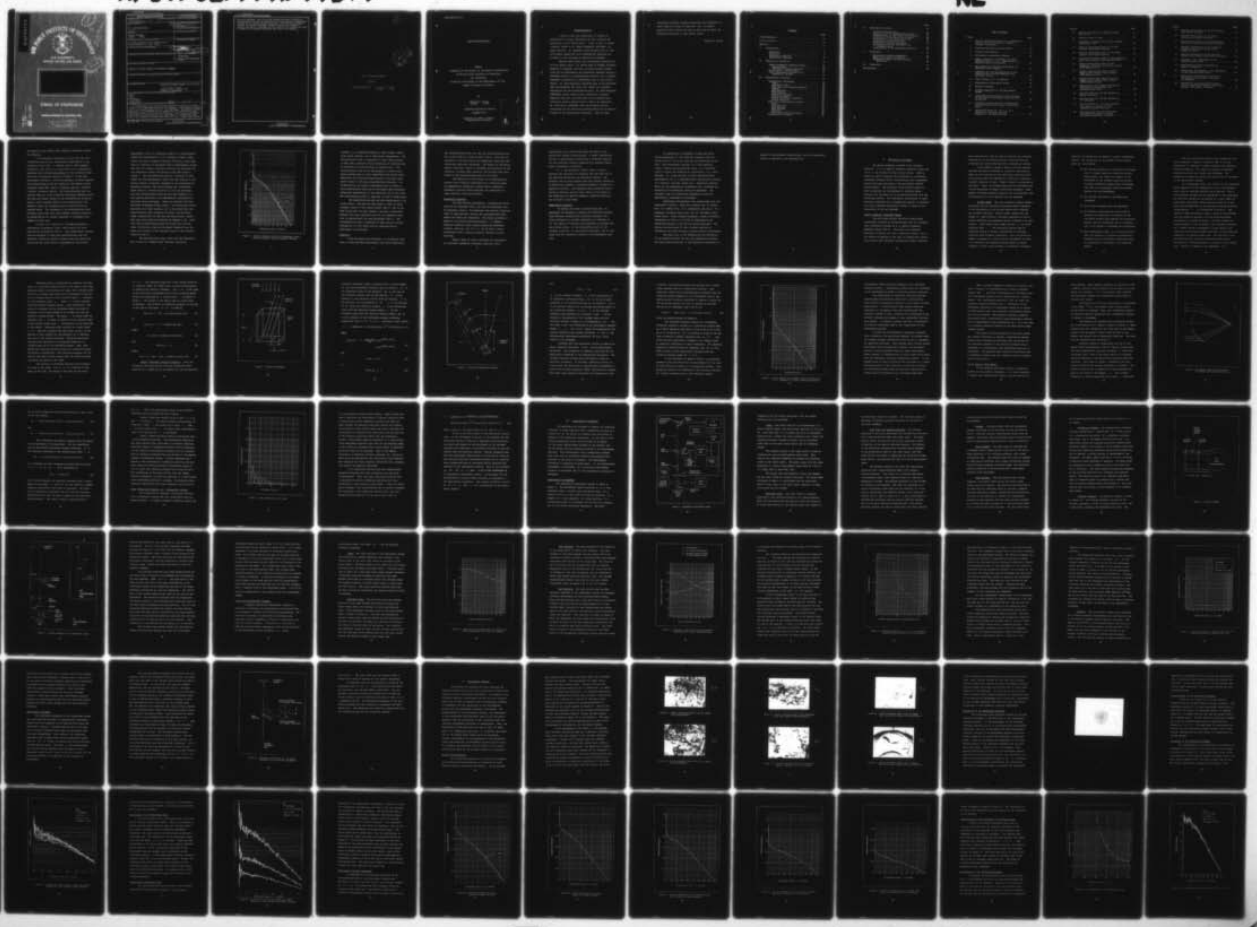

AIR FORCE INSTITUTE OF TECHNOLOGY

AIR UNIVERSITY
UNITED STATES AIR FORCE

SCHOOL OF ENGINEERING

WRIGHT-PATTERSON AIR FORCE BASE, OHIO

UNCLASSIFIED

SECURITY CLASSIFICATION OF THIS PAGE (When Data Entered)

REPORT DOCUMENTATION PAGE

READ INSTRUCTIONS BEFORE COMPLETING FORM

1. REPORT NUMBER: AFIT/GEP/PH/77D-7	2. GOVT ACCESSION NO.
3. RECIPIENT'S CATALOG NUMBER	
4. TITLE (and Subtitle): LASER AUTOREFLECTANCE,	5. TYPE OF REPORT & PERIOD COVERED: Master's thesis, MS Thesis
6. PERFORMING ORG. REPORT NUMBER	
7. AUTHOR(s): Charles W. Martin, Captain USAF	8. CONTRACT OR GRANT NUMBER(s)
9. PERFORMING ORGANIZATION NAME AND ADDRESS: Air Force Institute of Technology (AFIT-EN), Wright-Patterson AFB, Ohio 45433	10. PROGRAM ELEMENT, PROJECT, TASK AREA & WORK UNIT NUMBERS
11. CONTROLLING OFFICE NAME AND ADDRESS	12. REPORT DATE: Dec [redacted]977
	13. NUMBER OF PAGES: 97 (12) 109 p.
14. MONITORING AGENCY NAME & ADDRESS (if different from Controlling Office)	15. SECURITY CLASS. (of this report): Unclassified
	15a. DECLASSIFICATION/DOWNGRADING SCHEDULE

16. DISTRIBUTION STATEMENT (of this Report)

Approved for public release; distribution unlimited

17. DISTRIBUTION STATEMENT (of the abstract entered in Block 20, if different from Report)

18. SUPPLEMENTARY NOTES

Approved for public release; IAW AFR 190-17

JERRAL F. GUESS, Captain, USAF
Director of Information

19. KEY WORDS (Continue on reverse side if necessary and identify by block number)

Lasers
Light
Reflectance
Autoreflectance
Reflectivity

012 225

20. ABSTRACT (Continue on reverse side if necessary and identify by block number)

The autoreflectance peak in the angular reflectance distribution of laser radiation from nonspecular surfaces is investigated. An experimental apparatus using a He-Ne laser operating at 632.8 nm is described. This apparatus allowed measurement of the reflectance from a surface from 0° to 90° from the autoreflectance direction in the plane of incidence. The reflectance measurements from surfaces of (1) smoked MgO, (2) a $MgCO_3$ block, (3) a nonspecular gray paint, (4) a pigmented, polymeric bead paint, and (5) 3M Company Black Velvet

DD FORM 1 JAN 73 1473 EDITION OF 1 NOV 65 IS OBSOLETE

UNCLASSIFIED

SECURITY CLASSIFICATION OF THIS PAGE (When Data Entered)

paint are presented. Each of the five surfaces are shown to exhibit an autoreflectance peak and the dependence of the peak magnitude on measurement distance and the incidence angle is measured. A theoretical reflectance equation for coherent, collimated radiation indicent on a surface of spherical particles is developed, and the results of this equation are shown to compare to the measured reflectance data within a few percent.

LASER AUTOREFLECTANCE

THESIS

AFIT/GEP/PH/77D-7 Charles W. Martin
Captain USAF

AFIT/GEP/PH/77D-7

LASER AUTOREFLECTANCE

Thesis

Presented to the Faculty of the School of Engineering

of the Air Force Institute of Technology

Air University

In Partial Fulfillment of the Requirements for the

Degree of Master of Science

By

Charles W. Martin
Captain USAF

Graduate Engineering Physics

December 1977

Approved for public release;
distribution unlimited

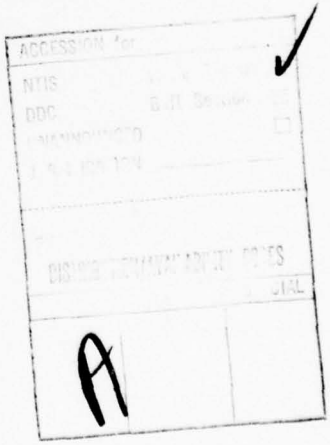

Acknowledgements

I wish to take this opportunity to express my appreciation to those individuals who have assisted and advised me in this thesis effort. First, I want to extend a special thanks to Dr. Robert Hengehold (AFIT/ENP), my thesis advisor. Dr. Hengehold saved me many hours of time with simple suggestions on my experimental approach and listened to and critiqued my theoretical arguments.

Several other people also contributed significantly to this thesis effort. Dr. Walter Egan of Grumman Aerospace Research in Bethpage, New York, provided valuable suggestions for my experimental and theoretical approach through a published article, a pre-publication article, and a personal telephone conversation as referenced later in the written thesis. Dr. Egan personally explained some of his published data and suggested the "glory ray" theory as a possible explanation for the autoreflection peak. Mr. Mike Moscynski (AFML/MBE) and Mr. Roger Vissoc (University of Dayton Research Institute) provided three of the nonspecularly reflecting surface samples which I used in my experiment. Mr. Cliff Kelto (AFML/MXA) took the scanning electron micrographs of the reflecting surfaces which are included as figures in the experimental discussion. Each of these

individuals provided valuable assistance and information in their respective areas of expertise, and I sincerely appreciate their taking the time to talk with me about the problems encountered in this thesis effort.

Charles W. Martin

Contents

List of Figures

Abstract

The autoreflectance peak in the angular reflectance distribution of laser radiation from nonspecular surfaces is investigated. An experimental apparatus using a He-Ne laser operating at 632.8 nm is described. This apparatus allowed measurement of the reflectance from a surface from 0° to 90° from the autoreflectance direction in the plane of incidence. The reflectance measurements from surfaces of (1) smoked MgO, (2) a $MgCO_3$ block, (3) a nonspecular gray paint, (4) a pigmented, polymeric bead paint, and (5) 3M Company Black Velvet paint are presented. Each of the five surfaces are shown to exhibit an autoreflectance peak and the dependence of the peak magnitude on measurement distance and incidence angle is measured. A theoretical reflectance equation for coherent, collimated radiation incident on a surface of spherical particles is developed, and the results of this equation are shown to compare to the measured reflectance data within a few percent.

LASER AUTOREFLECTANCE

I Introduction

Background

The fact that there is a sharp increase in the intensity of reflected electromagnetic radiation from a surface illuminated with nearly collimated radiation as the reflected radiation nears a propagation angle directly back along the incidence direction (near autoreflection) was first observed and reported by N. P. Barabashev in 1924. Barabashev noted a sharp increase in the brightness of the mare areas of the moon as the moon neared opposition; hence, this sharp autoreflectance peak has also been called the "opposition effect." In this thesis, this peak in the reflected radiation will be addressed as the autoreflectance peak.

A notable theoretical treatment of the lunar autoreflectance peak was published in 1963 by B. W. Hapke (Ref 4). In this article, Hapke develops a theory for reflection of radiation from a semi-infinite colloidal suspension of particles with inter-particulate shadowing. This theory successfully accounts for the lunar autoreflectance peak even though we know today that the lunar surface is not a colloidal suspension of particles. Hapke's derivation can

be applied to any surface where geometric shadowing effects are important.

It is extremely interesting to note that the autoreflectance peak was not conclusively demonstrated in the laboratory until 1966. P. Oetking (Ref 6) used wideband, collimated light from an arc lamp source in an experimental apparatus which allowed measurements of the reflected intensity from a reflecting surface to within 1° of the autoreflectance direction. With this apparatus, Oetking observed the autoreflectance peak for nearly all the samples tested including smoked MgO, which is commonly used as a standard "diffuse" reflector coating. The autoreflectance peak was clearly shown not to be a specular reflection component since the peak was always evident in the autoreflection direction even at large incidence angles to the statistically flat surfaces, where the incidence angle is defined from the surface normal. The existence of the autoreflectance peak obviously means that even such standard, diffuse reflectors as smoked MgO do not reflect radiation in accordance with Lambert's cosine law.

In 1976, W. G. Egan and T. Hillgeman proposed an experimental arrangement using a cube biprism for autoreflectance measurements (Ref 2). This experimental arrangement was designed to study the autoreflectance peak for different integrating sphere coatings since the autoreflectance peak may cause errors in hemispherical reflectance

measurements using an integrating sphere in a reflectometer. Reflectance measurements of flat coatings of $MgCO_3$, $BaSO_4$, sulfur and some 3M Company diffusely reflecting paints were made as a function of wavelength from a monochrometer source. Only data for normally incident radiation was published and the reflectance curves are typically like that shown in Figure 1. The autoreflectance peak as a function of wavelength for the monochrometer source was very similar to the earlier results of Oetking, extended to the autoreflection direction; however, Egan and Hillgeman then introduced a He-Ne laser as a source operating at 632.8 nm and found that the autoreflectance peak was much more dramatic for two surfaces which had a low hemispherical reflectance at the He-Ne laser wavelength. These two surfaces were blue and black 3M Company diffuse paints. No reflectance curves were given for these surfaces, but it was stated that the autoreflectance peak intensity was about five and seven times, respectively for the blue and black paints, larger than that which would be predicted by Lambert's law. Since this large autoreflectance peak was found only with the laser illumination, Egan and Hillgeman suggested that the effect was related to the coherence length of the incident radiation (Ref 2).

The autoreflectance peak, which has been demonstrated to exist for commonly used "diffuse" reflecting

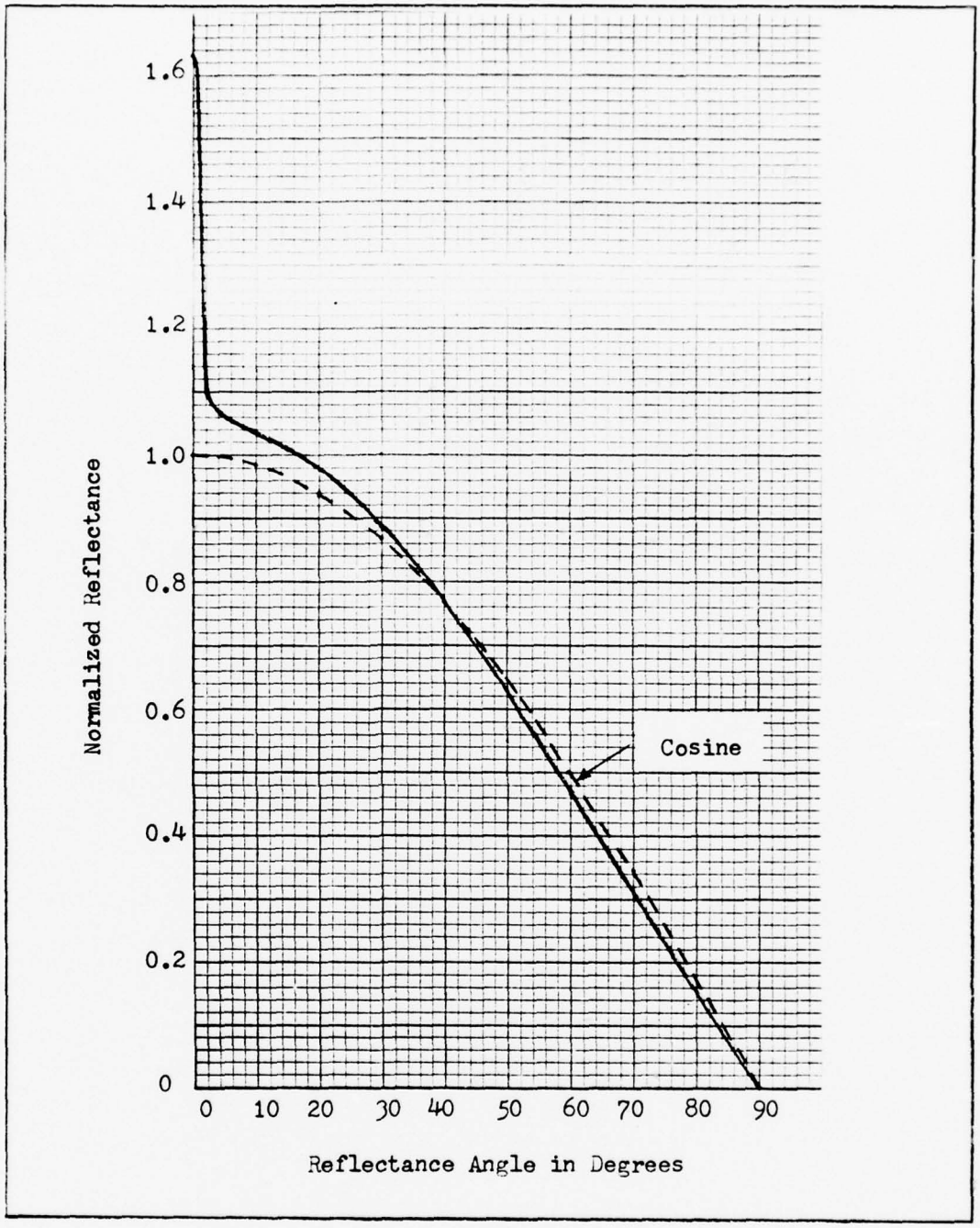

Figure 1. Typical Reflectance Curve for a Nonspecular Surface with Low Coherence, Normally Incident Irradiance

surfaces, is an important problem in laser safety, remote laser sensor systems, and in reflectance measurements. The autoreflectance peak is important to laser safety because in some cases, unusually large intensities of radiation may be reflected from such surfaces as painted walls. The autoreflectance peak may be advantageous to remote laser sensor systems such as laser rangefinders and active laser designator and tracking systems because of the high laser return signal in the near autoreflectance direction. As illustrated by the typical reflectance curve in Figure 1, the autoreflectance peak must be considered when performing reflectance measurements in the laboratory and in the field. The autoreflectance peak is important to each of these areas.

The autoreflectance peak has been demonstrated to be a real effect. The peak has been shown to exist at large incidence angles to the surface normal (Ref 5), and it has been stated that for some surfaces, the peak is much more dramatic for laser radiation than for low coherence radiation of approximately the same wavelength (Ref 2). The autoreflectance peak is important to many areas of optical engineering, so this effect must be characterized by measurement and explained.

Objective

From the background discussion, it is apparent that there is some published experimental data which demonstrate

the autoreflectance peak, but the only autoreflectance data for a laser source is found in Refs 2 and 3. This data is limited to a few data points for nonspecular reflectors and leaves many questions unanswered. The effects of reflecting surface structure, angles of incidence and reflection of the radiation, incident beam intensity, and incident beam wavelength on the autoreflectance peak are not known.

The objective of this effort is to experimentally analyze laser radiation reflectance for a selected number of nonspecularly reflecting surfaces and to formulate a radiometric function which describes the reflectance of laser radiation from such surfaces.

Theoretical Approach

For this written presentation, a theoretical discussion will be presented first, and then the experiment will be discussed; however, the experiment was actually conducted first to experimentally analyze the autoreflectance peak before the theory was formulated. The theory presented is based on two surface reflectance models: (1) Hapke's geometric shadowing model assuming perfectly incoherent incident radiation, and (2) H. C. van de Hulst's glory interference model assuming perfectly coherent incident radiation.

Hapke's model is used to describe the reflectance of collimated, perfectly incoherent radiation from a

statistically flat surface with gaps and holes in the particulate surface microstructure. A rough, hypothetical surface is approximately modeled and a governing equation for the reflected intensity measured by a proposed experimental arrangement is derived.

H. C. van de Hulst's "glory" model is used to describe the refraction of radiation into and back out of the particles which form the reflecting surface. The simplest case of glory scatter with one internal reflection is modeled for coherent, collimated radiation incident on a spherical particle. The resultant glory intensity distribution is derived, and the final result of the theory is the combination of Hapke's geometric shadowing model and van de Hulst's glory model.

Experimental Approach

To analyze the laser autoreflectance peak, an experiment was designed to measure the reflected intensity from different nonspecularly reflecting surfaces for a given wavelength of incident radiation as a function of (1) the angles of incidence and reflectance as defined from the surface normal, (2) the polarization state of the incident radiation, (3) the surface irradiance, and (4) the range from the reflecting surface to the measurement aperture.

An experimental arrangement is described which allows measurement of the reflected intensity from the surface from 0° out to 90° from the autoreflectance direction. This arrangement utilizes (1) a long coherence length, linearly polarized He-Ne laser, (2) a half-wave plate to rotate the direction of polarization, (3) a beam expander, (4) a beam splitter to allow autoreflectance measurements and (5) a photomultiplier tube detector mounted on a rotating, variable length rail. Sensitivity measurements for the experimental arrangement and a technique for determining the background signal are presented. The procedure used for reflectance measurements with this experimental arrangement is discussed.

Reflectance measurements were accomplished with five nonspecular surfaces. These five surfaces are (1) smoked MgO, (2) a $MgCO_3$ block, (3) a nonspecular gray paint, (4) a pigmented, polymeric bead paint, and (5) 3M Company Black Velvet paint. These surfaces represent a range of relative reflectance of from 1.0 to 0.025 as referenced to the smoked MgO surface at the 632.8 nm He-Ne wavelength. The surface microstructure of each of these materials is documented with field emission scanning electron micrographs.

The final step is the presentation and discussion of the measured results for the five nonspecular surfaces. The final equation derived in the theoretical discussion is

applied to the polymeric bead surface, and this theoretical result is compared to the measured data.

II Theoretical Discussion

The theory presented is based on two existing theories: (1) B. W. Hapke's geometric shadowing theory and (2) H. C. van de Hulst's glory scatter theory. Hapke's theory is used to describe the reflectance of collimated, incoherent radiation from a statistically flat nonspecular surface with gaps and holes in the particulate surface microstructure. Van de Hulst's glory scatter theory is used to describe the interference of radiation which refracts into and back out of the particles which form the reflecting surface. The reflectance distribution of laser radiation reflected from a nonspecular surface, as measured by a finite aperture measurement system, is shown to be a combination of the two theories.

Hapke's Geometric Shadowing Theory

The only known surface reflection theory which successfully predicts an autoreflectance peak for nonspecularly reflecting surfaces is B. W. Hapke's geometric shadowing theory (Ref 4). This model was originally developed to explain the lunar "opposition effect," but it can readily be applied to any type of nonspecularly reflecting surface with incoherent collimated incident radiation.

This equation will later be used to describe the intensity envelope for an interference pattern resulting from the reflectance of laser radiation from a nonspecular surface.

A few changes to Hapke's theory are made; however, the same derivation procedure as originally published by Hapke can be followed with the same final reflected intensity equation when the assumption of perfectly incoherent incident radiation is used. Hapke's theory is presented in two parts. First, the surface model will be developed with a brief discussion of Hapke's derivation procedure. Then, Hapke's reflected intensity equation will be presented, and the predictions of this equation will be examined.

Surface Model. The only difference between Hapke's derivation and the following reflectance model discussion is the description of the surface medium which reflects the incident radiation. Hapke's model assumes that the medium is a semi-infinite, colloidal suspension of microscopic scattering and absorbing objects arranged in an open network. These objects have number density n and cross-sectional area σ. The scattering objects must be separated enough to prevent interference of radiation reflected from different scatterers. Here the reflecting medium is modeled as a semi-infinite arrangement of radiation scattering and absorbing objects which are bound together to form a solid surface, so perfectly incoherent

radiation is assumed for the moment to negate interference effects. The assumptions to be applied in this surface model are listed below.

(1) The surface consists of a semi-infinite arrangement of roughly spherical scattering objects. These objects are large with respect to the wavelength of the incident radiation and are arranged irregularly enough within the medium such that on a macroscopic scale the surface appears flat and homogeneous.

(2) The incident radiation is collimated and incoherent.

(3) Only singly scattered rays are important.

(4) An effective scattering law can be used to describe the reflection of radiation of the individual objects that comprise the reflecting medium, and this scattering law is a function only of the angles of incidence and reflectance.

(5) Where absorption occurs, it is continuous such that the intensity of radiation exponentially decreases with an extinction coefficient which is proportional to distance in the absorbing medium.

The only differences between these assumptions and those presented in Hapke's derivation (Ref 4) are the assumptions of incoherent incident radiation and spherical scattering objects. The reason for assuming incoherent incident radiation has already been discussed. The assumption of spherical scattering objects will be discussed in the experimental results.

On a macroscopic scale, the surface of the reflecting medium appears flat and homogeneous, but on a microscopic scale, only an effective surface can be defined. Only a flat effective surface will be considered in this discussion. The effective surface can be modeled as a large number of microscopic tubes whose cross-sectional areas are of the same order-of-magnitude as the individual scattering object cross-sections, σ , as illustrated in Figure 2. The length of these microscopic tubes is equal to the distance into the effective surface a ray can penetrate before encountering a scattering object. The tube lengths are always parallel to the direction of the incident radiation. For a random surface arrangement of these objects, the tubes will have various lengths from zero to many times the diameter of an average object size. The idea that a ray can penetrate well into the reflecting medium before encountering a scattering object is crucial to this discussion. Figure 2 is shown in two dimensions. In a

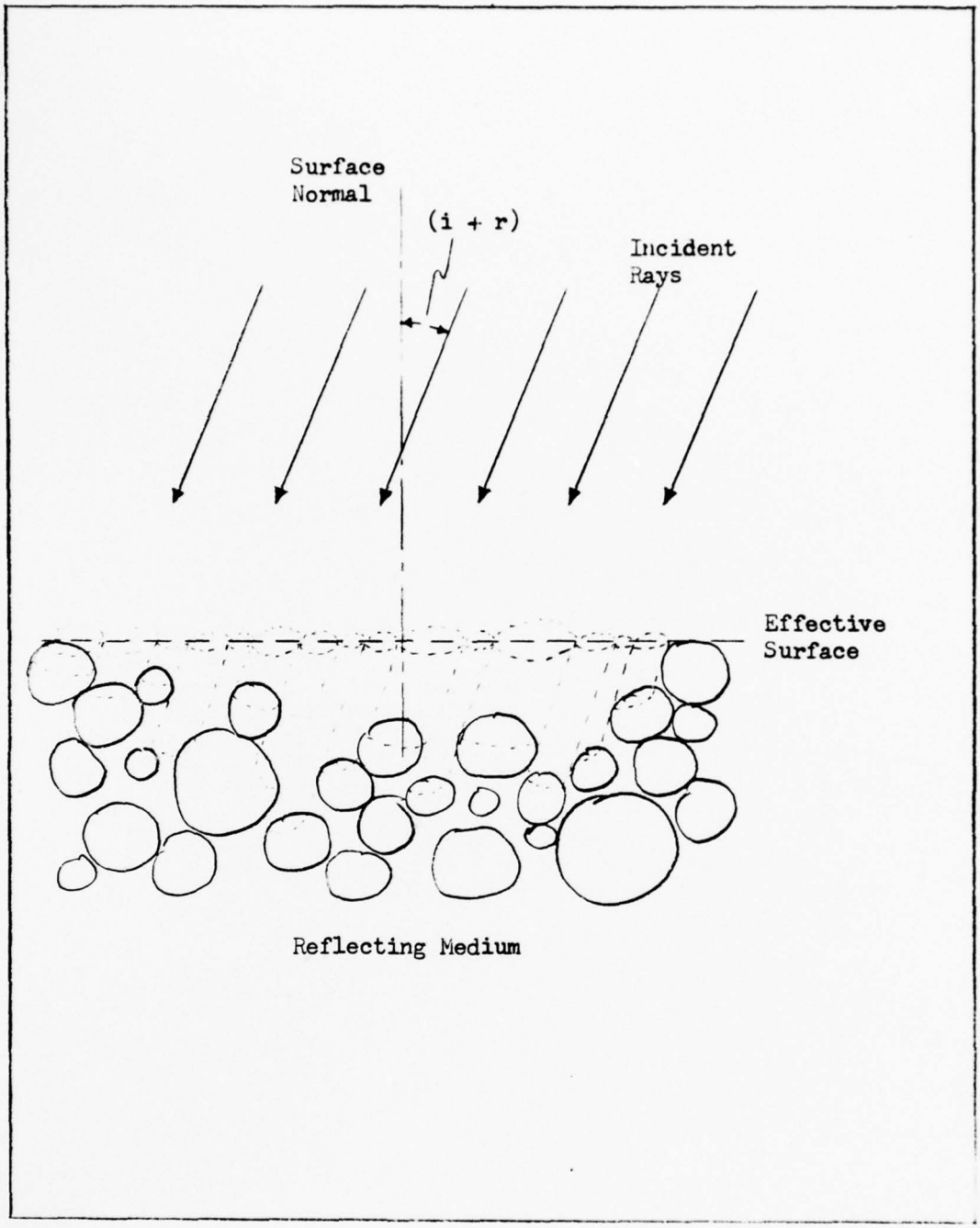

Figure 2. Idealized Reflecting Surface Model

three-dimensional representation, there can be many tubes through the outer layer of individual objects even though these objects may be bound together to form a real surface.

Now consider a particular tube through the effective surface. Light can pass through the tube and scatter from the object at the end of the tube. The scattered radiation can travel back out the end of the tube without encountering any other scattering objects, but the radiation scattered into the imaginary wall of the tube has a finite probability of encountering another scatterer.

An incident beam of collimated radiation whose beam diameter is orders of magnitude larger than the average scattering object size will be attenuated as it penetrates beyond the effective surface according to the expression

$$I = I_o e^{-z/\tau \cos i} \qquad (1)$$

where I is the intensity at a distance z below the effective surface, I_o is the intensity at the effective surface, τ is the distance over which the beam is attenuated by the factor e, and i is the angle of incidence as defined from the normal to the effective surface. This expression assumes a continuous scattering process which is expected to be a valid approximation over a distance which is large with respect to the individual scattering object size.

Radiation which is reflected can intersect the tube walls or it can pass directly back out the ends of the tubes. Radiation which is reflected at an angle that intersects the walls of an average area tube will be attenuated on the way out in a manner similar to Eq 1 with the angle i replaced by the reflection angle r, where r is again defined from the effective surface normal. Only reflection in the plane of incidence will be considered where the plane of incidence is the plane formed by an incident ray and the effective surface normal. The angle i is always taken as positive, and r is taken as positive on the opposing side of the surface normal from i and negative on the same side of the normal. Radiation which reflects at a small angle $(i + r)$ does not intersect the tube walls, so Eq 1 is not applied to this fraction of the radiation as it reflects back out of the reflecting medium. Radiation which does intersect the tube walls is attenuated further as it reflects back out of the reflecting medium. Thus, even though the scattering objects within the reflecting medium may scatter isotropically, that radiation escaping out the ends of the tubes is more intense than the radiation which intersects the walls of the tubes.

The fraction of reflected radiation which escapes the ends of the tubes, $F(z, i, r)$, is a function of the shape of the tube, the length of the tube and the angle

$(i + r)$. The imaginary tubes for a real surface would be of irregular shape, but Hapke chose a square cross-section to simplify the analytic treatment. $F(z, i, r)$ is the same as the fractional overlapping area of two rectangles whose centers are displaced by $z \tan(i+r)/\cos i$, as shown in Figure 3. The bottom of the square tube is always fully illuminated. The fraction of radiation escaping out the end of the tube at the angle $(i + r)$ is given by

$$F(z,i,r) = [y^2 - yz \tan(i+r)/\cos i]/y^2 \qquad (2)$$

or

$$F(z,i,r) = 1 - z \tan(i+r)/y \cos i \qquad (3)$$

where

$$0 \leq (i+r) \leq \arctan [(y \cos i)/z] \qquad (4)$$

and

$$F(z,i,r) = 0 \qquad (5)$$

where

$$(i+r) < 0 \quad \text{and} \quad (i+r) > \arctan [(y \cos i)/z] \qquad (6)$$

Hapke's Reflected Intensity Equation. Using the fractional term given by Eq 3 and the attenuation term given by Eq 1, Hapke set up an equation for the differential

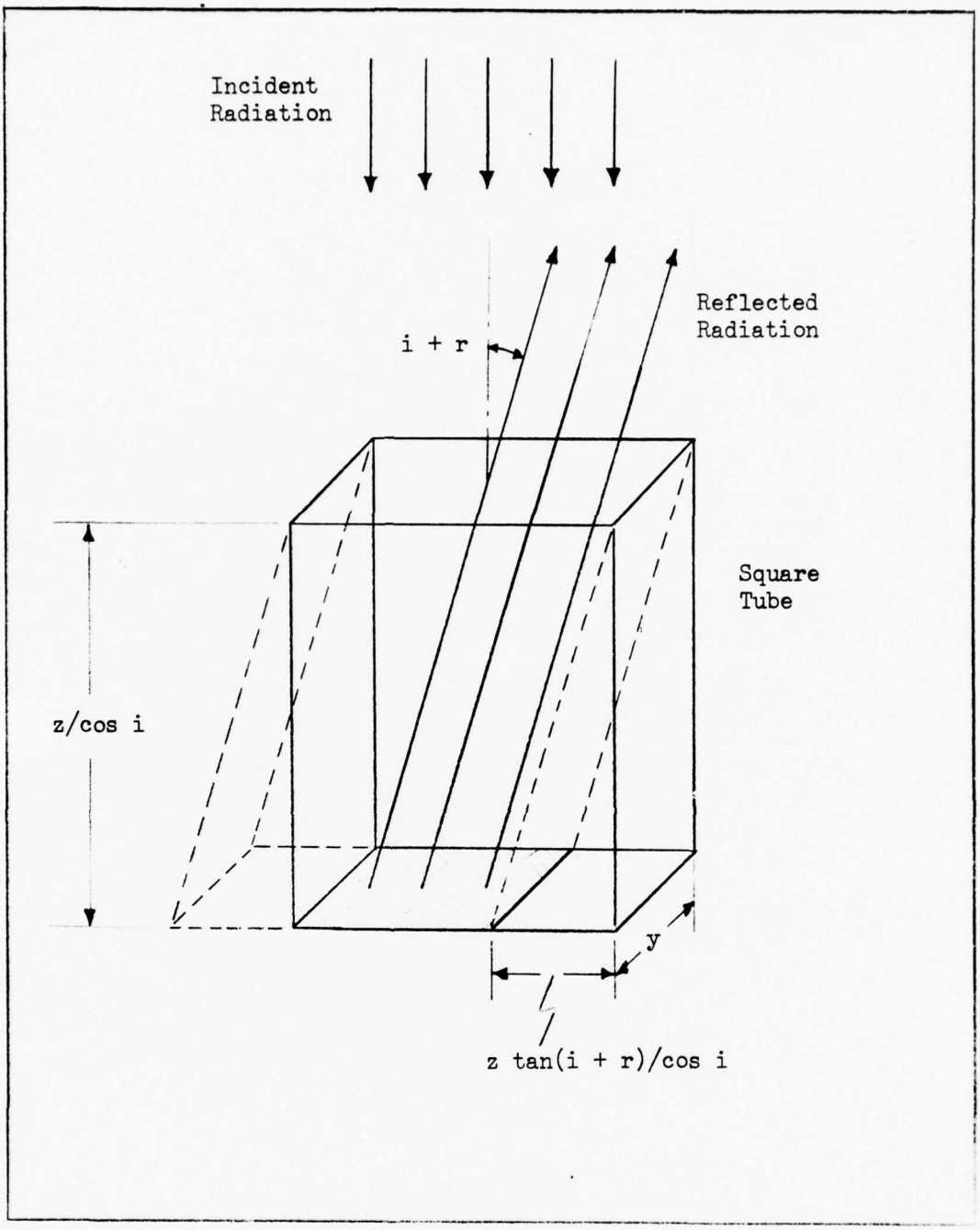

Figure 3. Surface Tube Geometry

intensity reflected toward a detector from a volume element dV with the measurement geometry shown in Figure 4. $d\omega$ is the acceptance angle of the detector, dA is the area of the effective surface seen by the detector, R' is the distance to the effective surface from the detector, R is the distance from the detector to dV , z is the distance of dV below the effective surface, r is the reflectance angle from the effective surface normal, i is the incidence angle from the effective surface normal, and I_o is the intensity of the collimated incident radiation. Integration from R = R' to R = ∞ resulted in (Ref 4:4575)

$$I = I\, bd\Omega dA \cos|r| \,(1+\cos|r|/\cos i)^{-1}\, S(i+r)H(i+r,g) \quad (7)$$

where

$$H(i+r,g) = 2 - \frac{\tan|i+r|}{2g}\,[1-e^{-g/\tan|i+r|}]\,[3-e^{-g/\tan|i+r|}] \quad (8)$$

for

$$|i+r| \leq \pi/2 \quad (9)$$

or

$$H(i+r,g) = 1 \quad (10)$$

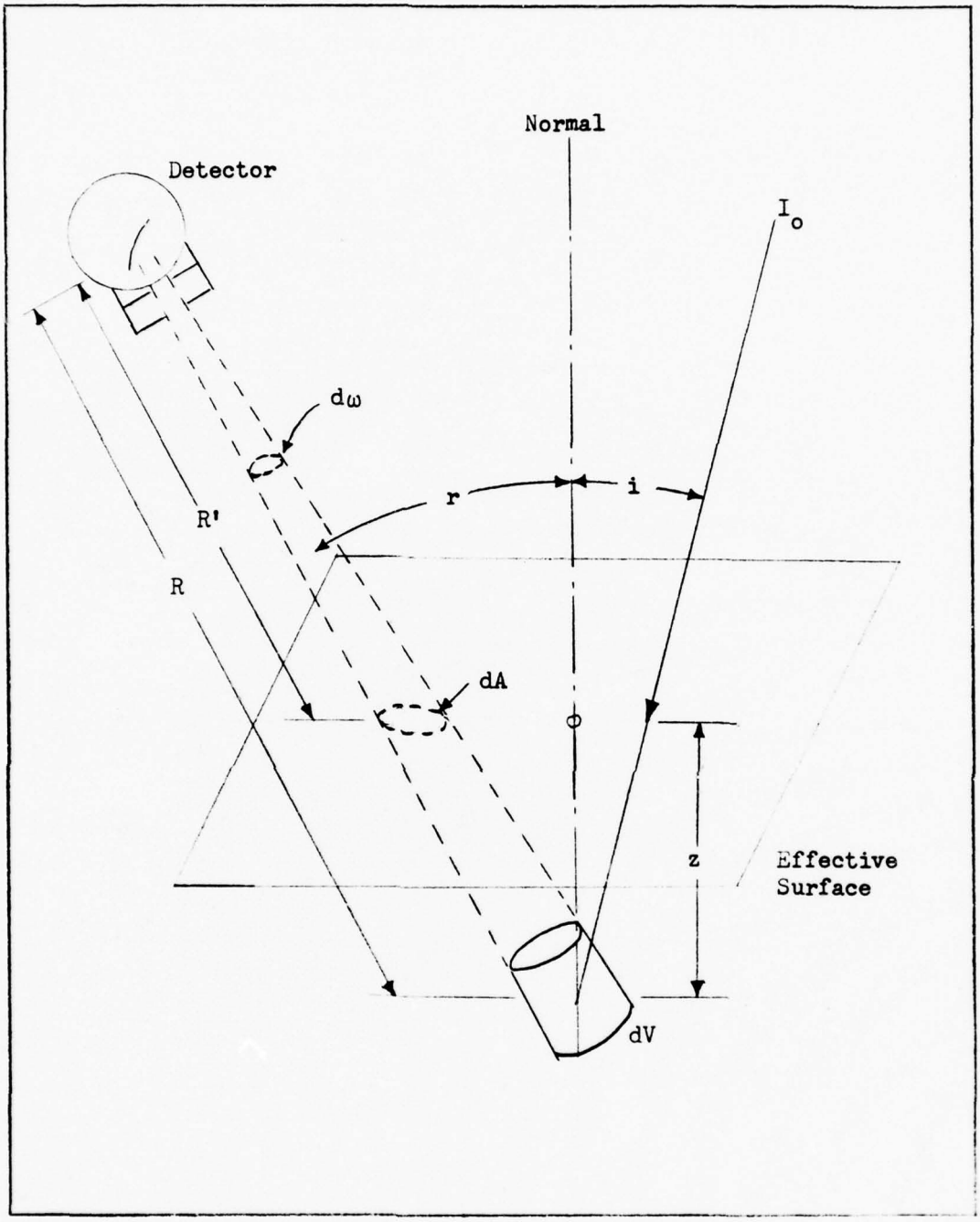

Figure 4. Reflectance Measurement Geometry

for

$$|i+r| \geq \pi/2 \tag{11}$$

I_o is the incident intensity, b is the reflectivity of an individual scattering object, $d\Omega$ is the solid angle subtended at the effective surface by the detector, S(i+r) is the scatter function for an average scattering object in the reflecting surface, $g = y/\tau$, y is the average shadowing tube dimension as in Figure 3, and τ is the distance of penetration of the incident beam into the effective surface to where it is attenuated by 1/e. All the terms in Eq 7 are determined by the measurement geometry except b, g, and S(i+r) which are determined by the surface reflecting the incident radiation. b and g are experimentally measureable quantities, so only S(i+r) remains to be discussed.

Assuming that the nonspecular surface is made up of small, spherical particles, S(i+r) can be analytically determined. The assumption of spherical particles will be specifically addressed in the experimental discussion. The incident radiation treated here with Hapke's theory is perfectly incoherent. An isolated, spherical particle of a size where ray optics may be applied would be expected to scatter the incident radiation almost isotropically; however, when these small spherical particles are compacted to form

a surface, the effective scattering function for a single sphere becomes more of a backscatter function. This compaction result may be approximated by assuming that the elemental surface segments of the illuminated side of the sphere scatter radiation according to Lambert's cosine law. The scattering pattern for such an assumption has been worked out by Schoenberg (Ref 7:111-2) as

$$S(i+r) = [\sin |i+r| + (\pi-|i+r|)\cos |i+r|]/\pi \qquad (12)$$

using the angles defined in Figure 4.

The reflected intensity pattern for collimated, incoherent radiation incident on a reflecting surface made up of small spherical particles is thus given by Eq 7 with Eqs 8 or 10 and Eq 12. Eq 7 is plotted in Figure 5 for the case of normally incident radiation with $g = 0.1$. The curve has been normalized to Lambert's law (dashed curve) by numerical integration in three dimensions. The radiation apparently reflected from the elemental area dA of this model surface is thus spherically diverging with the intensity envelope shown for $g = 0.1$.

In the discussion of Hapke's theory, a significant assumption was made which must be reconsidered for the case of laser radiation incident on a nonspecular surface. This assumption involves the coherence of the incident radiation. For incident radiation with a long coherence length,

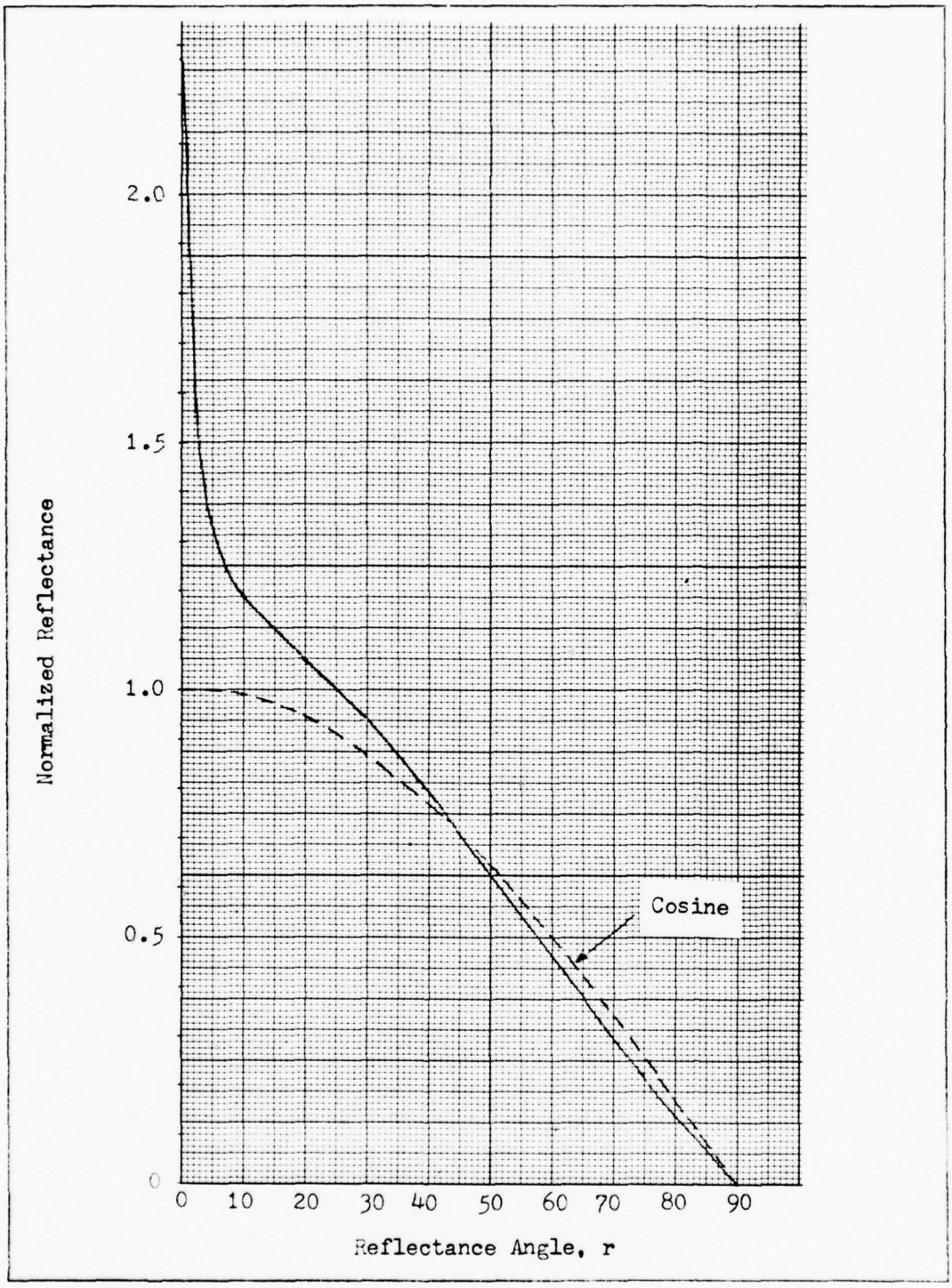

Figure 5. Hapke's Equation for Normally Incident Radiation with g = 0.1 Normalized to a Perfect Lambertian Reflector

interference effects would be expected in the reflected radiation pattern. Interference effects were not considered in the development of Hapke's reflected intensity equation.

The interference of radiation reflected from the assumed spherical particles which form a statistically rough surface as depicted in Figure 2 is not easily treated analytically. A statistically rough surface which has variations in the depth of the real surface below the effective surface of only a fraction of a wavelength of the incident radiation can present a very complicated interference pattern. A realistic surface also has a distribution of particle sizes which adds to the complication of the interference pattern.

To treat the interference of radiation scattered from a surface of the particulate spheres, an ordered array of in-phase coherent oscillators could be used to represent the spherical particles. This ordered array of point source oscillators can be analytically treated, and the result would be a nearly periodic series of sharp interference peaks; however, an ordered array of point source oscillators does not represent a realistic nonspecular surface. If the ordered array of point oscillators was perturbed to a random distribution with a wide variation in oscillator spacing, the interference peaks would be much more numerous with a random angular distribution and a decreased amplitude.

When a surface composed of spherical particles like that in Figure 2 is considered with a surface roughness greater than λ and with a distribution in the sphere size, the interference pattern will be complicated in a similar manner. The interference peaks will "fill in" under the intensity envelope defined by Eq 7. Therefore, if the measurement aperture of a measurement system as in Figure 4 is sufficiently large, the individual interference maxima will not be resolved. The measured reflected intensity distribution with a sufficiently large measurement aperture will be approximately that described by Eq 7, as in the case of incoherent radiation incident on the same surface model assumed earlier.

The result of this discussion is that even though the incident radiation is coherent, interference effects arising from reflection of radiation from the surface of the individual spheres of the reflecting surface can be neglected if a sufficiently large measurement aperture is considered. The measured laser radiation reflectance from a nonspecular surface with this condition would be approximately given by Eq 7.

Van de Hulst's Glory Theory

If the spherical particles forming a nonspecular surface are not perfect conductors, it is also reasonable to expect that radiation can refract into and back out of

these spheres. When coherent radiation is incident on such a sphere, radiation which refracts into and back out of the sphere can interfere. H. C. van de Hulst (Ref 7:249-58) has previously treated this interference effect which is often called "glory."

The analysis of the glory interference is approached in two steps. First, the simplest case of glory from a single sphere is examined. Then, the interference pattern of coherent radiation reflected from a nonspecular surface of spheres is discussed.

The simplest ray diagram which illustrates scatter due to refraction into a sphere is shown in Figure 6. Three parallel rays are incident on the right side of the sphere, refract into the sphere, reflect from the rear of the sphere, and refract into a backscatter direction. The final rays are diverging from the point 0.

Coherent radiation illuminating one side of the sphere could thus generate a ring of "source" points along the curve generated by revolving the point 0 around the horizontal axis. Such a ring would result in a toroidal wavefront emerging in the backscatter direction which can interfere. The circle in Figure 7 represents the focal circle from which the toroidal wavefront is emerging. The radius of this circle is assumed to be approximately the same as the radius of the sphere, a. The incident radiation is linearly polarized at an angle Ψ referenced

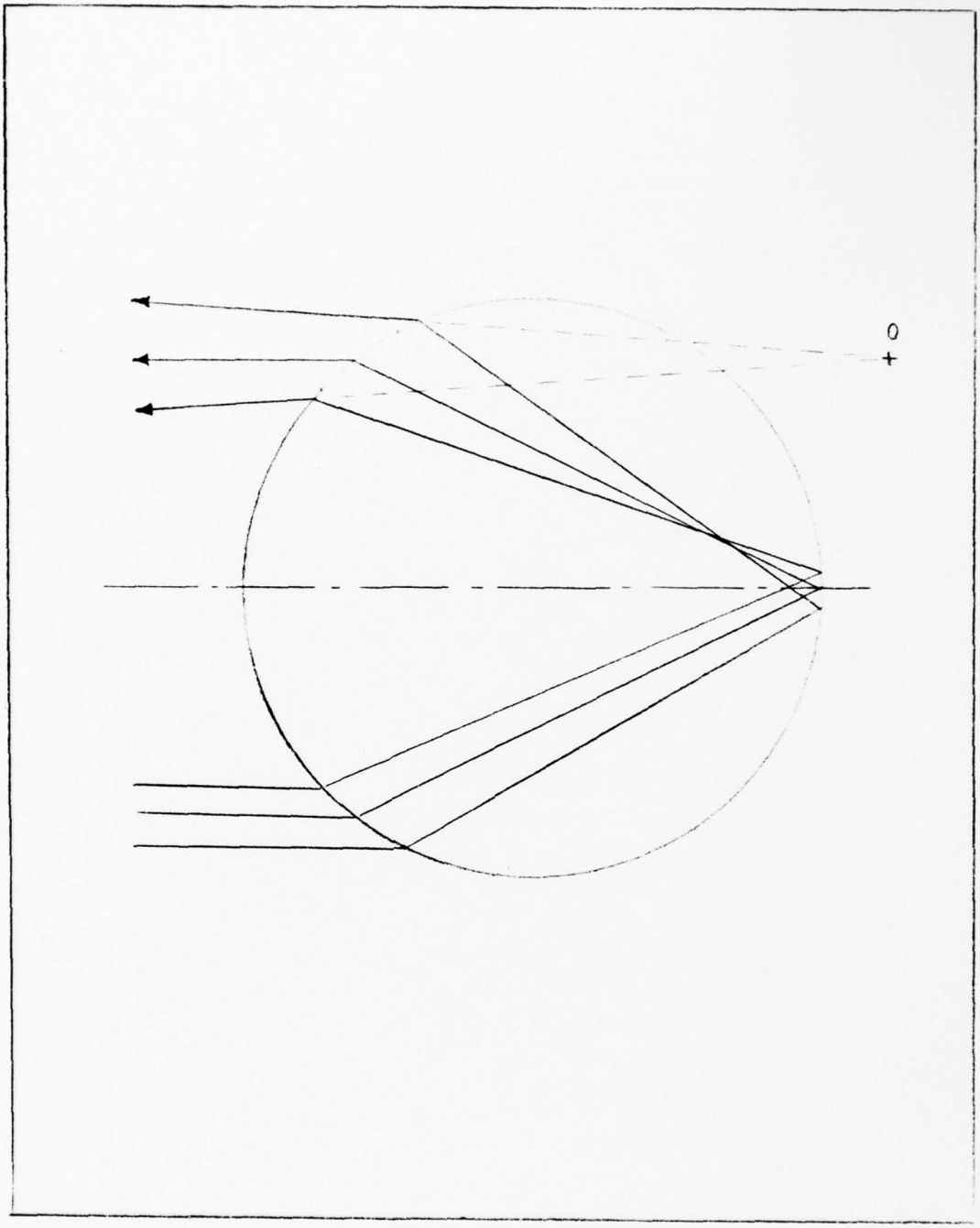

Figure 6. Ray Diagram Illustrating Backscatter of Radiation from a Sphere (Ref 7:250)

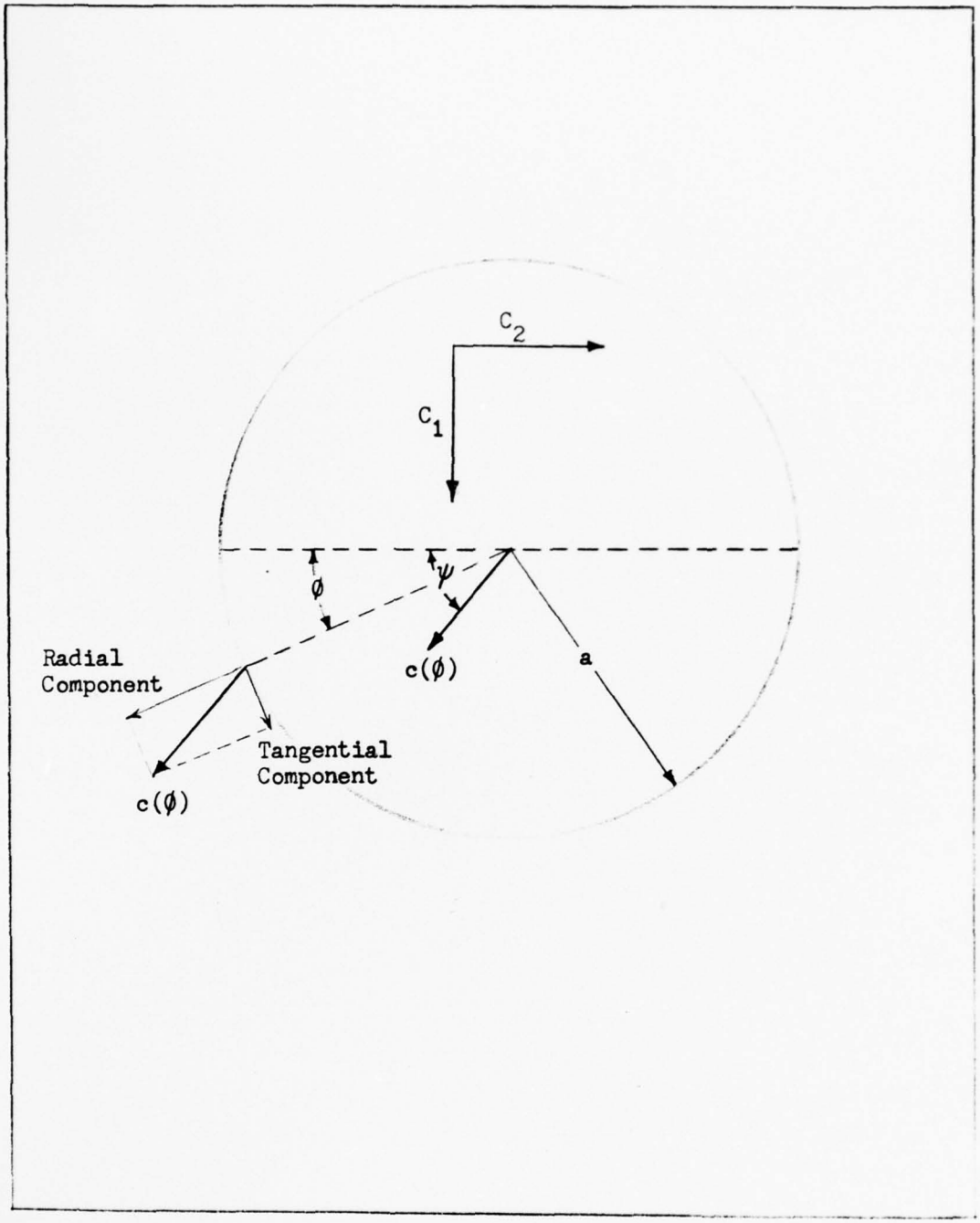

Figure 7. Schematic for the Decomposition of the Electric Field Vectors Emergent from the Focal Circle (Ref 7)

to the plane of incidence which is the plane of Figure 6 (indicated by the dashed line in Figure 7). The radiation vector $c(\phi)$ emerging from a point on the circle specified by the angle ϕ consists of two components with the amplitudes $B_1 \cos(\psi-\phi)$ in the radial direction and $B_2 \sin(\psi-\phi)$ in the counterclockwise tangential direction. B_1 and B_2 are proportional to ε_1 and ε_2 for the material of the sphere. To determine the amplitude vectors of the total wave at the assumed small angle r from the sphere axis in the plane of incidence, the emerging vector at all points around the circle must be decomposed into components perpendicular and parallel to the plane of incidence. Respectively, these are

$$C_1(\phi) = (B_1\cos^2\phi+B_2\sin^2\phi)\sin\psi - (B_1-B_2)\sin\phi\cos\phi\cos\psi \quad (13)$$

and

$$C_2(\phi) = (B_1-B_2)\sin\phi\cos\phi\sin\psi - (B_1\sin^2\phi+B_2\cos^2\phi)\cos\psi \quad (14)$$

Using the substitution $u = \sin(2\pi ar/\lambda) \simeq 2\,a|r|/\lambda$, the amplitudes of the emergent radiation are

$$A_{1,2} = \frac{1}{2\pi}\int_0^{2\pi} e^{-iu\cos\phi} C_{1,2}(\phi)\, d\phi \quad (15)$$

Eq 15 can be integrated with the substitution of Eqs 13 and 14 for the results

$$A_1 = \tfrac{1}{2} \sin \psi \{B_1[J_0(u)-J_2(u)] + B_2[J_0(u)+J_2(u)]\} \quad (16)$$

and

$$A_1 = \tfrac{1}{2} \cos \psi \{B_1[J_0(u)+J_2(u)] + B_2[J_0(u)-J_2(u)]\} \quad (17)$$

The intensities are readily computed from the square of the magnitude of the amplitudes. For the simplifying case of horizontally polarized incident radiation, $\psi = 0$, the intensity scattered at the dimensionless angle u is

$$I(u) = \tfrac{1}{4} \left| B_1[J_0(u)+J_2(u)] + B_2[J_0(u)-J_2(u)] \right|^2 \quad (18)$$

It is expected for most nonspecular surface materials that $\varepsilon_1 = \varepsilon_2$, so $B_1 = B_2$. Eq 18 simplifies to

$$I(u) = B^2 \left| J_0(u) \right|^2 \quad (19)$$

Eq 19 is the intensity of radiation scattered from a single sphere at the angle $u \simeq 2\pi a|r|/\lambda$ for the coherent incident radiation polarized in the plane of incidence. The radiation is spherically divergent with the intensity envelope defined by Eq 19, and its peak is always in the autoreflectance direction. The glory is wholly unpolarized with

$B_1 = B_2$. Thus, the polarization state of the incident radiation does not affect the glory scatter.

Figure 8 shows the results of Eq 19 with $a = 5$ μm and $\lambda = 0.6328$ μm . The glory intensity distribution is broad for a small u and narrow for a large u . When a is much greater than λ , the small angle approximation used in the equation for u is satisfied.

Figure 8 shows the glory scatter distribution from a single spherical particle. The interference effects of the glory scatter from a multitude of different spherical particles forming a nonspecular surface would be identical to that argued in the previous discussion of the interference of radiation reflected from the surface of the spheres forming a nonspecular surface. Surface roughness and a spread in the distribution of spherical particle size will again cause any multiple particle interference maxima to fill in under the intensity envelope curve given by Eq 19. The interference of the glory scatter from the random surface arrangement can again be neglected if a sufficiently large measurement aperture is assumed. The measured glory intensity distribution with this assumption will be Eq 19.

Final Reflectance Equation for a Nonspecular Surface

The reflectance of coherent, collimated radiation from a nonspecular surface has been investigated with two separate models: (1) Hapke's geometric shadowing theory and

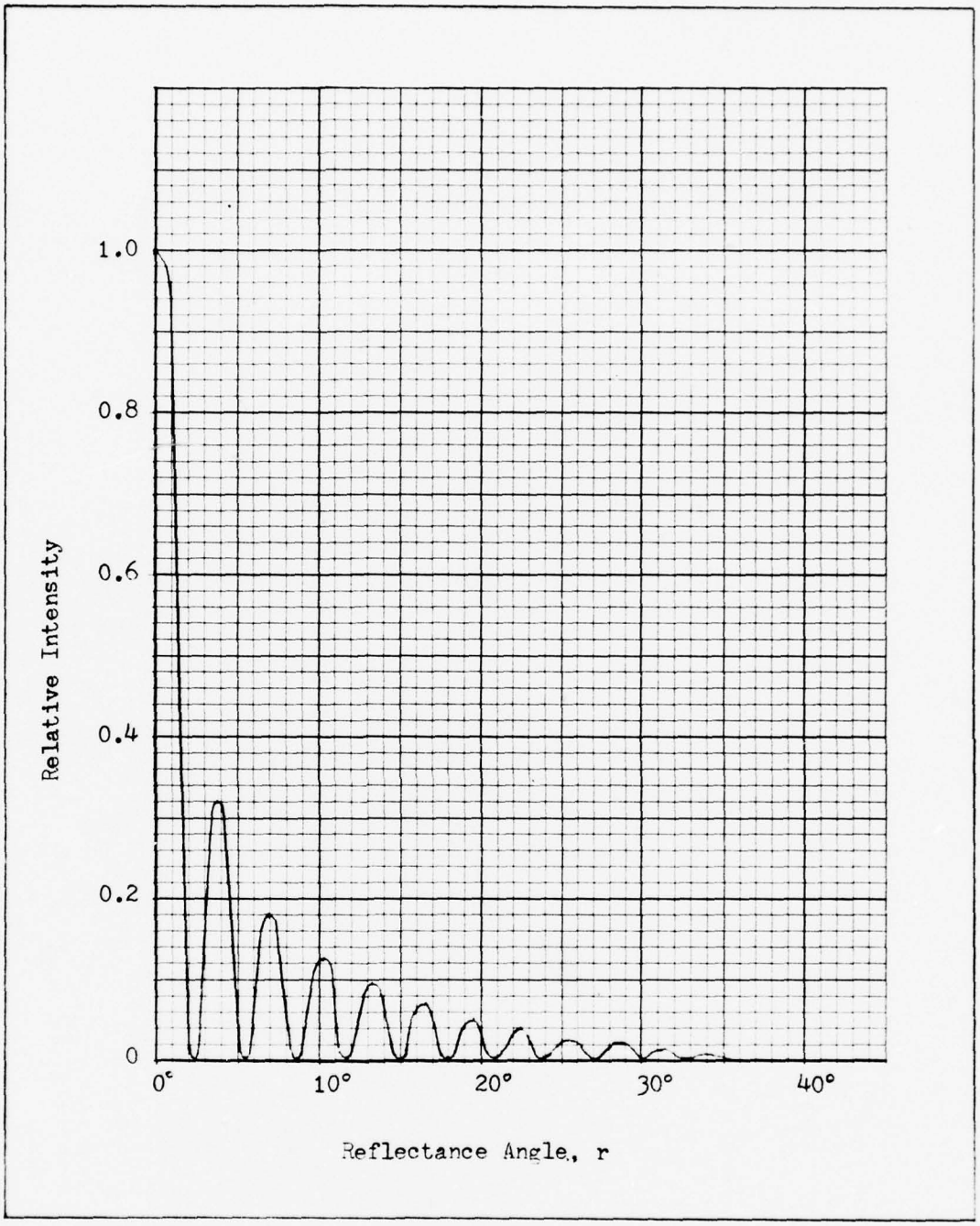

Figure 8. Glory Scatter for a 5 μm Sphere

(2) van de Hulst's glory scatter theory. Hapke's model was used to describe the reflectance of coherent radiation from a statistically rough nonspecular surface with gaps and holes between the spherical particles forming the surface. Van de Hulst's glory scatter model was used to describe the interference of radiation from refraction into and back out of the spherical particles which form the nonspecular surface. Both models used the assumption of a sufficiently large measurement aperture such that the interference peaks of the radiation scattered from a large number of spherical particles could not be resolved. Each of the models resulted in a reflected intensity envelope, Eq 7 and Eq 19, which would be measured by this sufficiently large measurement aperture for laser radiation reflecting from a nonspecular surface of spherical particles.

It is intuitively obvious that both geometrically shadowed scattering and glory scattering can take place simultaneously. Thus, the total reflected intensity from a nonspecular surface of spherical particles will be a combination of the results of both models. Since the terms may be assumed to be noninterfering due to surface roughness and variations in the spherical particle size, the total measured reflectance will be the sum of Eqs 7 and 19.

$$I = I_o d\Omega dA \cos|r| \left[\frac{\sin|i+r| + (\pi-|i+r|)\cos|i+r|}{\pi}\right]$$

$$\{b[1+\cos|r|/\cos i]^{-1} H(i+r,g)+B^2|J_0(2\pi a|r|/\lambda)|^2\} \qquad (20)$$

where $H(i+r,g)$ is given by Eq 8 or 10, and $g = y/\tau$.

Eq 20 is the final result of the theoretical discussion. In the development of Eq 20, it was assumed that the reflecting surface is made up of spherical particles which are large with respect to the wavelength of the incident radiation and rough with a statistical variation of the real surface from the effective surface. Another assumption was that the measurement aperture must be sufficiently large so that multiple particle interference maxima are not resolved. These assumptions must be considered before applying this equation to any experimental results. Each of the variables I_o , $d\Omega$, dA , r , i , and λ in Eq 20 are determined by an experimental measurement system. An experiment for the determination of each of these variables is presented in the experimental discussion. The surface variables in Eq 20 (b , B^2 , a , y , and τ) will be discussed in the experimental results.

III Experimental Discussion

The experiment was designed to measure the reflected intensity of laser radiation from a nonspecular surface as a function of (1) the angles of incidence and reflectance as defined in the theoretical discussion, (2) the angle of the linear polarization state from the plane of incidence, (3) the total radiant power incident on the surface, and (4) the range from the reflecting surface to the measurement aperture. Only statistically flat, nonspecular surfaces were used, and all reflected intensity measurements were confined to the plane of incidence. The experimental discussion is presented in three parts: (1) the experimental arrangement is described, (2) a sensitivity measurement analysis is discussed, and (3) the experimental procedure is discussed.

Experimental Arrangement

The experimental measurement system is shown in Figure 9. The measurement system consisted of (1) a long coherence length, linearly polarized He-Ne laser, (2) a half-wave plate, (3) beam power and spectrum monitors, (4) a chopper, (5) a beam expander, (6) a beam splitter, (7) a reflecting surface to be studied, (8) the detector assembly, and (9) the signal processing components. The above

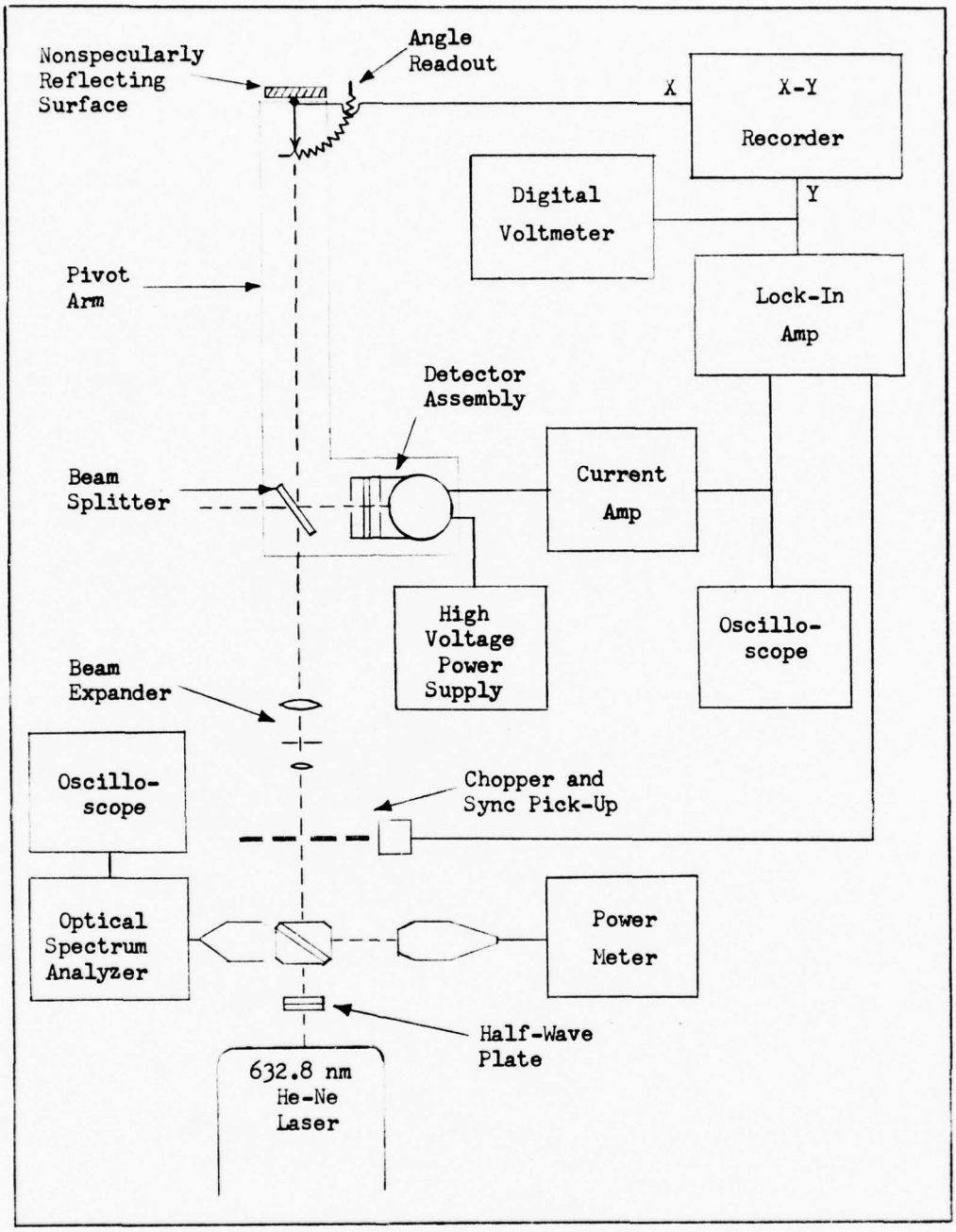

Figure 9. Experimental Measurement System

components will be briefly described, then the system operation will be discussed.

Laser. The source used for all measurements is a Spectra-Physics Model 125A He-Ne laser operating at 0.633 μm, CW. This laser has a 1.8 m plasma tube with an adjustable output mirror, a Model 325 cavity extension with a Model 585 coherence extender (tuneable etalon), and an adjustable prism used as the final cavity mirror and for frequency tuning.

The tuneable etalon in the laser cavity is used to eliminate all but one longitudinal cavity mode. This reduces the frequency bandwidth and extends the coherence length of the laser output. The power output with the laser operating in a single longitudinal cavity mode at 0.633 μm in a TEM_{oo} mode is less than 3 mW.

The plasma tube uses Brewster's angle end windows, and the laser output is linearly polarized. The output beam divergence is about 0.7 milliradian and the beam waist, which is very close to the laser output aperture, is about 2 mm across the $1/e^2$ points.

Half-Wave Plate. The laser output is linearly polarized in the vertical direction, so a Spectra-Physics Model 310 half-wave plate was used to rotate the direction of linear polarization to any desired angle with respect to

the horizontal plane of incidence. The half-wave plate is graduated in degrees and mounts directly to the front of the laser assembly.

Beam Power and Spectrum Monitors. The relative magnitude of the total beam power was continuously monitored with a Spectra-Physics Model 401C power meter. The power monitor signal was derived from optical component surface reflections in the optical spectrum analyzer. The portion of the beam power reflected into the power meter depended on the polarization angle of the laser output, but this power monitor was useful in observing the variation of beam power during a reflectance data scan at a fixed polarization angle.

The spectral output of the laser was continuously monitored with a Spectra-Physics Model 470-1 Optical Spectrum Analyzer. This device is a scanning Fabry-Perot interferometer with a free spectral range of 2 GHz and a bandwidth of 20 MHz. The maximum resolution is thus 20 MHz, full width at half maximum. The laser was operating in a single longitudinal mode which was not resolved, so it can only be stated that the coherence length of the laser was greater than or equal to about 15 m. A small percentage of the beam was reflected into the optical spectrum analyzer with a flat plate dielectric beam splitter. The optical spectrum analyzer was used to insure that the laser spectral

characteristics did not significantly change during the measurements.

Chopper. A Keithley Model 8403-225 synchronous chopper was placed in the beam path to chop the beam at 225 Hz. With the internal synchronizing signal from the chopper, the output from the photomultiplier detector could thus be synchronously amplified with a lock-in amplifier.

Beam Expander. The laser beam was expanded and collimated using a Jodon spatial filter with a 10X microscope objective, a 25 μm pinhole aperture, and a glass collimating lens. The emergent beam size could be changed by substituting different focal length collimating lenses. Using different diameter collimated beams, the reflecting surface irradiance could be varied with a relatively constant total beam power.

Beam Splitter. The beam splitter was a 28 mm diameter, 3 mm thick, fused silica flat with a first surface gold film coating. The gold film was deposited on the beam splitter substrate using an in-house, tungsten filament evaporation system. Enough gold was deposited on one side of the substrate to achieve 50% transmission through the beam splitter with the beam splitter surfaces at a reflection angle of near 45° in the horizontal plane with a horizontally polarized beam. The gold coated side

of the beam splitter was always facing the detector at a 45° angle.

Reflecting Surfaces. The nonspecularly reflecting surfaces studied were (1) smoked MgO, (2) a $MgCO_3$ block, (3) a nonspecular gray paint, (4) a pigmented, polymeric bead paint, and (5) 3M Company Black Velvet paint. The smoked MgO surface was prepared by burning research grade magnesium ribbon in air beneath a 25 mm diameter steel disc. The burning ribbon was constantly moved around beneath the disc to deposit a uniform coating of approximately 1 mm thickness. The $MgCO_3$ sample used was a 7 cm by 7 cm block of medicinal grade carbonate of magnesia. The $MgCO_3$ block was prepared by gently rubbing an area of the block flat with a fingertip. The three painted surfaces were prepared by the Air Force Materials Lab, Elastomer and Coatings Branch. The paints are each a two component type paint where a pigmented binder was sprayed onto a surface and then the second pigmented agent was sprayed on. The paint samples were each coated on three separate 25 mm diameter steel discs.

Detector Assembly. The detector assembly is shown in Figure 10. The detector assembly consisted of two circular apertures, a 0.633 μm narrow bandpass filter, and an EMI 9781R (extended red) photomultiplier tube. The

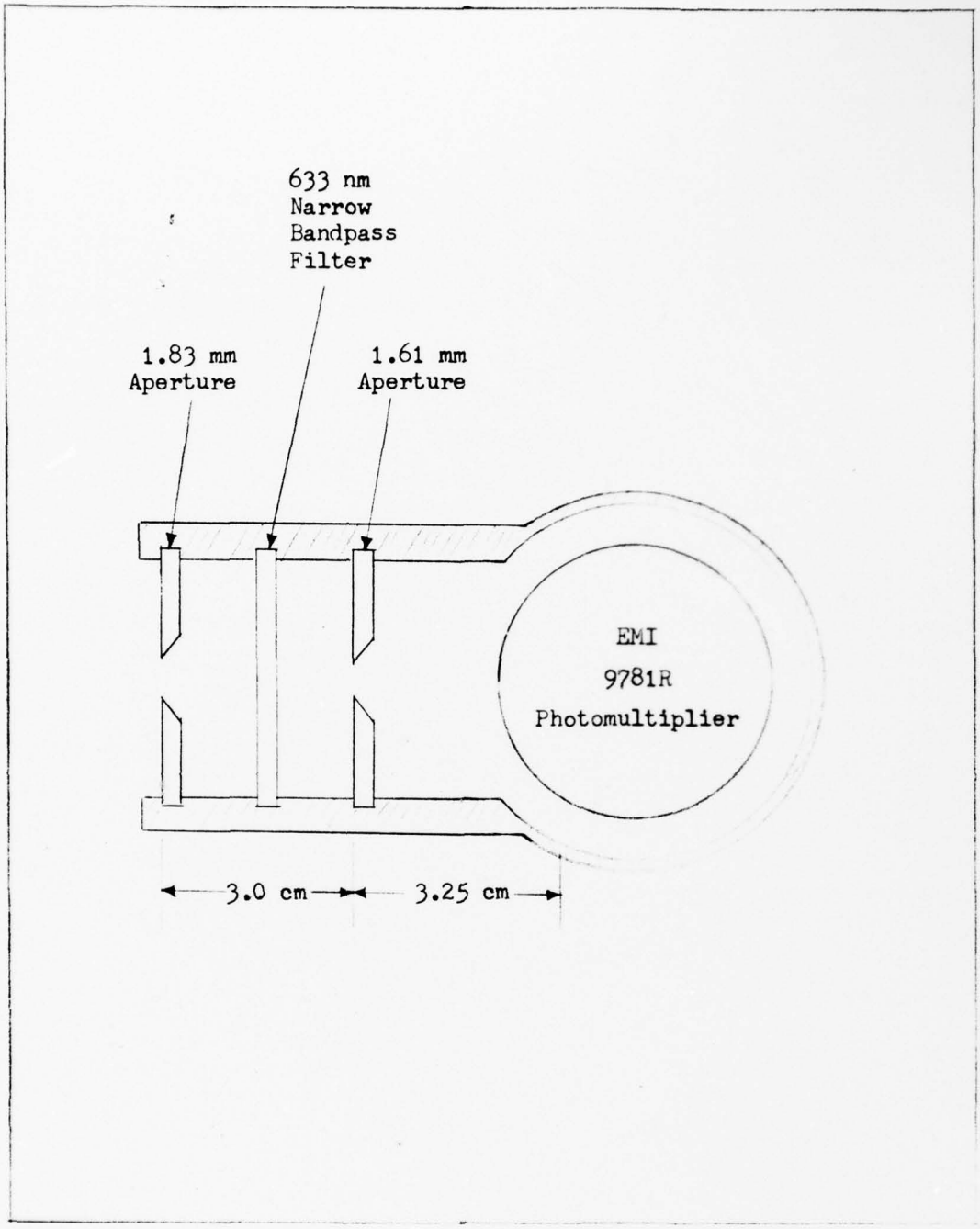

Figure 10. Detector Assembly

apertures limit the field-of-view of the detector to the area of concern on the reflecting surface and also reduce the solid angle subtended by the detector from the reflecting surface. The narrow bandpass filter reduced the sensitivity of the detector to extraneous background radiation other than the reflected 0.633 μm laser radiation. The EMI 9781R photomultiplier tube was selected for its extended red response and small dark current at room temperature operation. The response linearity and field-of-view of this detector assembly are discussed in the experimental sensitivity analysis.

Signal Processing Components. The current signal from the photomultiplier tube detector was first amplified by a Keithley Model 427 current amplifier. The current amplifer output was DC coupled to a monitor oscilloscope and AC coupled to a Model 407 Autoloc synchronous amplifier. A synchronizing signal was obtained directly from the chopper. The DC lock-in amplifier output was damped with a 1 second time constant and parallel coupled to a digital voltmeter and the Y-input of an X-Y recorder. The Y scale thus represents the radiant power incident on the photomultiplier detector. The X scale of the X-Y recorder was calibrated in degrees using a potentiometer readout of the angle $(i+r)$.

System Operation. The optical components of the measurement system are shown in Figure 11. The plane of Figure 11 is horizontal. The laser, half-wave plate, beam expander, and reflecting surface positions were fixed on a large, flat table. The reflecting surface was mounted vertically with a retaining clip against the top edge of the surface substrate on a mechanical stage which translated in a direction parallel to the reflecting surface. This stage was mounted on a second stage which rotated about a vertical axis along the reflecting surface. The incidence angle, i, could be independently varied by rotating the reflecting surface, and different areas of illumination on the surfaces could be selected by translation parallel to the surface.

The beam splitter and the detector assembly were mounted on a triangular base optical bench, 1 m long, which could be pivoted about an axis at the end of the triangular bench directly beneath the laser beam spot on the reflecting surface. This axis was coincident with the rotation axis of the reflecting surface. A potentiometer was geared from this fixed axis to measure the pivot angle, $i+r$, of the sliding triangular bench. The beam splitter and the detector assembly were attached to the same transverse adjustable triangular base mount, but the centers of the beam splitter and the detector assembly were separated by 8 cm in a direction perpendicular to the triangular bench. The beam

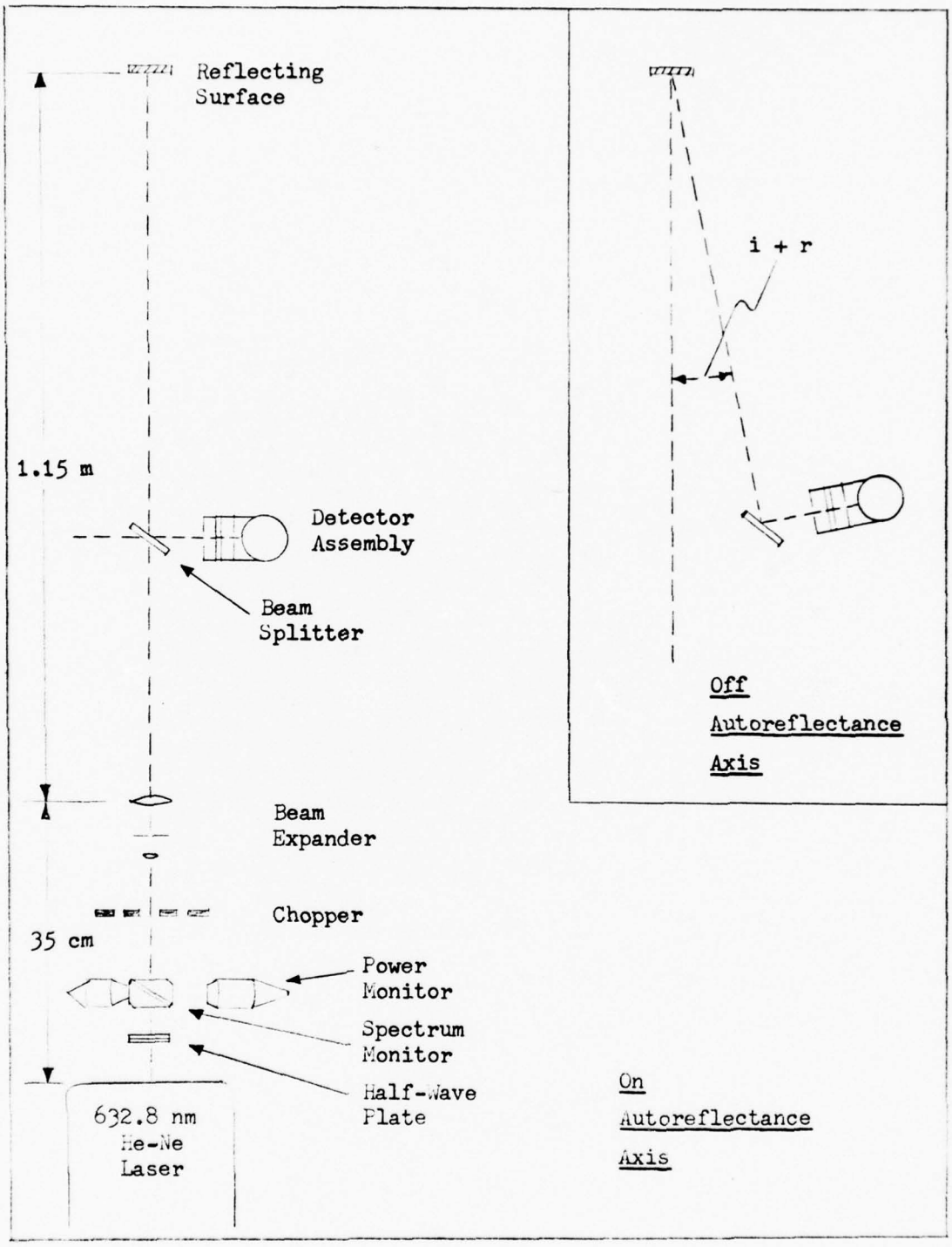

Figure 11. Primary Components of the Measurement System

splitter was mounted on the upper end of a pin mount in a lens holder. An 8 cm offset bracket connected the beam splitter pin mount to a pin mount for the detector assembly. The detector assembly shown in Figure 10 was mounted on two mechanical stages. The lower stage was for one-dimensional horizontal translation, and the second was a vertical axis rotation stage. These two stages were used to align the detector assembly.

The linearly polarized laser beam emerging from the half-wave plate of Figure 11 was expanded and collimated by the beam expander. When $i+r = 0$, the beam split at the beam splitter with 50% of the power transmitting to the reflecting surface to be studied and the rest of the power specularly reflecting out into the laboratory. The "split" part of the incident beam was not used for any part of the experiment. The radiation scattered from the nonspecular reflecting surface in the autoreflectance direction (back up the beam) again encountered the beam splitter. Part of this scattered radiation transmitted through the beam splitter back along the beam and was attenuated by the beam expander. A portion of the scattered radiation reflected from the gold coated side of the beam splitter into the detector. This irradiance at the detector was the quantity to be measured.

The incident beam passed through the beam splitter toward the reflecting surface only when the reflectance

measurement angle was small (about 2.5° for a beam splitter to reflecting surface distance of about 50 cm). At an angle dependent on the beam splitter to reflecting surface distance, the incident beam hit the edge of the beam splitter. A technique to avoid any measurement error due to laser beam scatter from the beam splitter edge will be discussed in the experimental procedure. At a measurement angle larger than the angle to the beam splitter edge, the incident beam traveled directly to the reflecting surface with an increase in surface irradiance. A constant percentage of the radiation incident on the beam splitter from the nonspecularly reflecting surface was deflected into the detector assembly. Thus, a complete scan of the measurement angle, $0 \leq |i+r| \leq \pi/2$, could be accomplished in two segments with this measurement system.

Sensitivity Measurement Analysis

A complete sensitivity measurement analysis is presented to determine the experimental factors which must be considered to analyze the reflectance measurements. The sensitivity analysis is presented by considering the principal optical components of Figure 11 individually and then the system alignment. Sensitivity is used here to describe the performance dependence of any system component on the measurement system variables; i.e., linear

polarization angle, the angle i+r , and the measured reflected intensity.

Laser. The laser position in the measurement system was fixed and all system components were aligned on the output beam, so the only laser factor to consider is the power output. The power output of the laser was continuously monitored with the Model 401C power meter. A maximum variation of about 4% in the laser output power between different reflectance scans was attained by adjusting the laser between scans back to a maximum output level between scans. The maximum variation of laser output during a single scan was less than 4%. The laser generally required more than one hour of warm up time before the required stability could be achieved.

Half-Wave Plate. The half-wave plate was mounted directly on the laser housing and directly affected the laser output power as a function of linear polarization angle. This dependence of power output on the polarization angle is shown in Figure 12. The data were measured by placing a power meter directly behind the half-wave plate in the beam and recording the power as a function of polarization angle as defined from the horizontal. The variation was apparently caused by front and rear surface reflections from the half-wave plate feeding back into the laser cavity through the Brewster windows on the plasma tube.

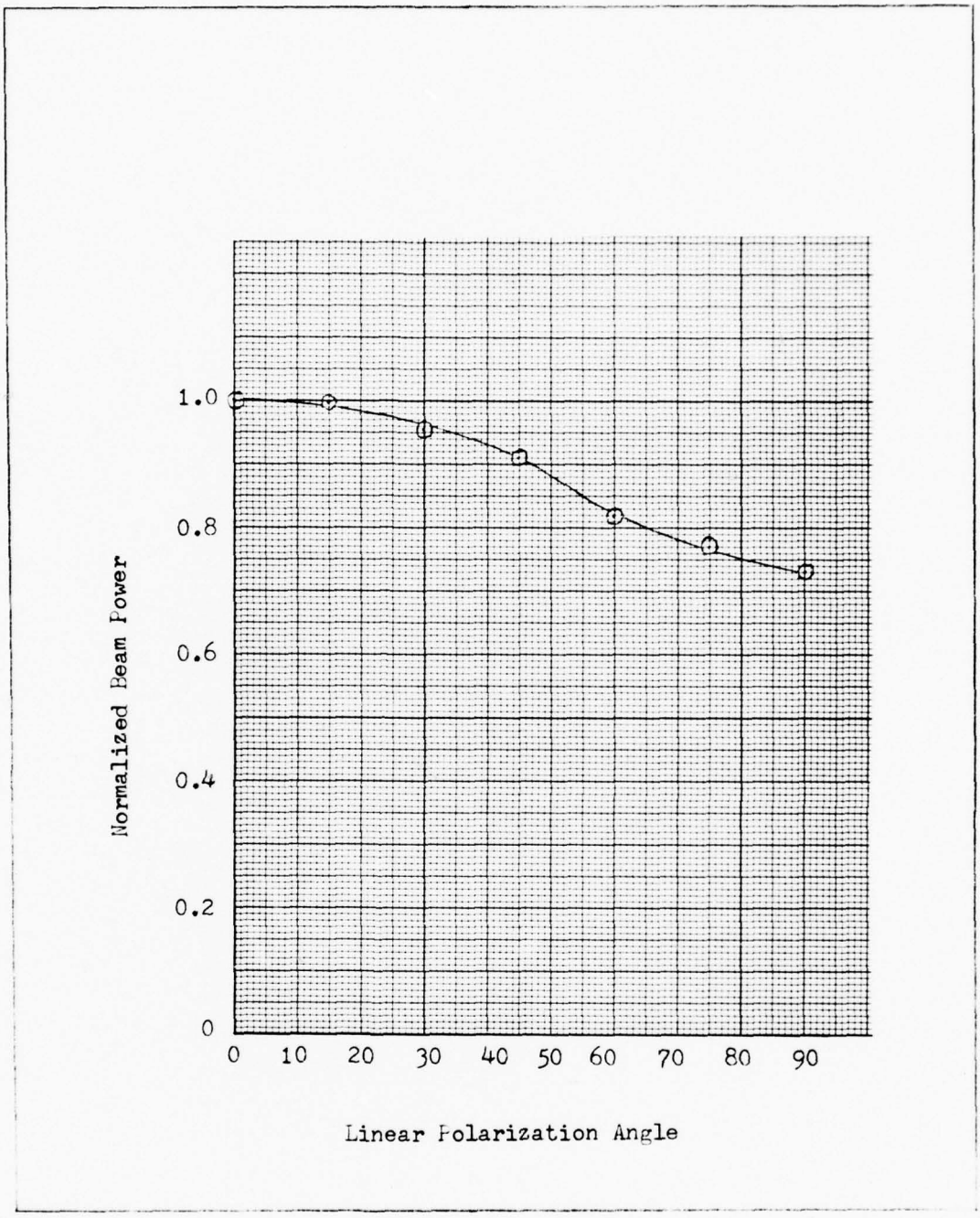

Figure 12. Laser Beam Power Variation with the Angle of the Linear Polarization State from the Horizontal

Beam Expander. The beam expander was not sensitive to any experimental variables but alignment. The lens elements of the beam expander and the pinhole had to be accurately aligned to obtain a collimated beam which emerged coincident with the axis of the input beam. The focus of the converging lens was adjusted such that the central diffraction disc of the focused beam just overfilled the 25 μm pinhole, then the collimating lens was adjusted to obtain the longest possible Rayleigh range. The minimum expanded beam diameter (with the 25.4 mm focal length collimating lens) was about 4 mm at the $1/e^2$ points.

Beam Splitter. The beam splitter was the most important component in the measurement system for reflected intensity measurements at near autoreflectance angles. Since the beam splitter was a thin gold film on a dielectric substrate and was oriented at approximately 45° to the incident beam, variation in the transmittance and reflectance of the beam splitter for different linear polarization angles was expected. This variation is shown in Figure 13 where the dependence of laser output with polarization angle as shown in Figure 12 has been removed by normalizing the data to a constant beam power reference level. The lower curve in Figure 13 was obtained by placing a 1/20 wave mirror at the nonspecular reflecting surface position normal

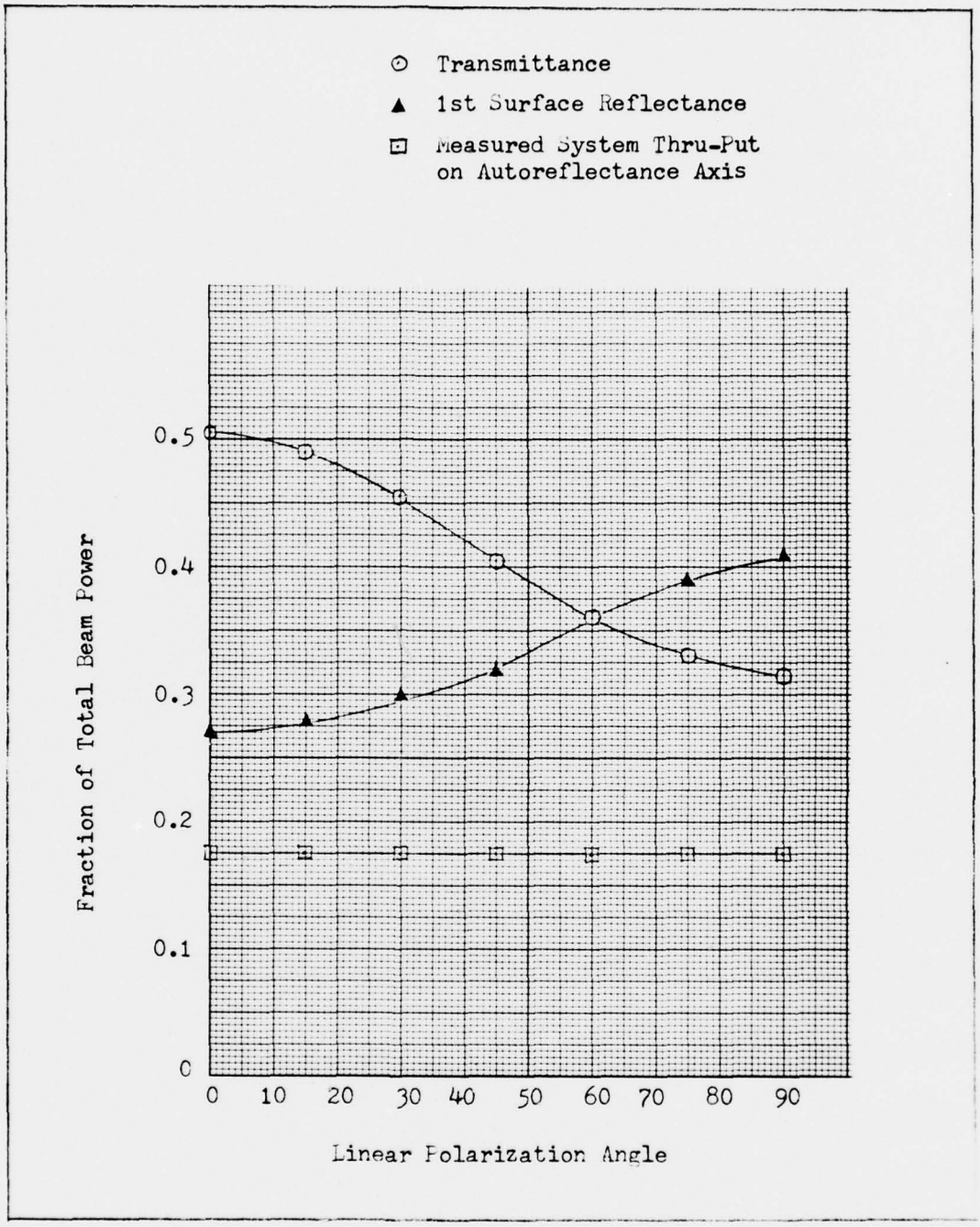

Figure 13. Variation of Beam Splitter Transmittance and Reflectance with Linear Polarization Angle

to the beam and measuring the radiant power at the detector position.

The incidence angle on the beam splitter changed as $45°-|i+r|$. The angle between the beam splitter and the detector was fixed at 45°, but the transmission through the beam splitter to the reflecting surface changed only slightly with the small incidence angle change. At the smallest beam splitter to reflecting surface distance, the incidence angle changed a maximum of 2.5° before the edge of the incident beam touched the edge of the beam splitter. The measured transmittance of the beam splitter decreased less than 4% over this range, so the beam splitter transmittance dependence on the angle $i+r$ was ignored.

A final measurement factor of the beam splitter to be considered is that a small amount of radiation was scattered from the beam by the beam splitter surfaces. The scatter from the coated side of the beam splitter was the most significant and could be seen by an observer's eye when the laboratory area was darkened. This beam splitter scatter presented a background signal to the detector when the scatter spot of the incident beam was within the field of view of the detector. Figure 14 illustrates this scatter for $i+r = 0$ as a function of distance. Two steel discs coated with lampblack from a fuel rich oxygen-natural gas flame were used to block the two beams emerging from the

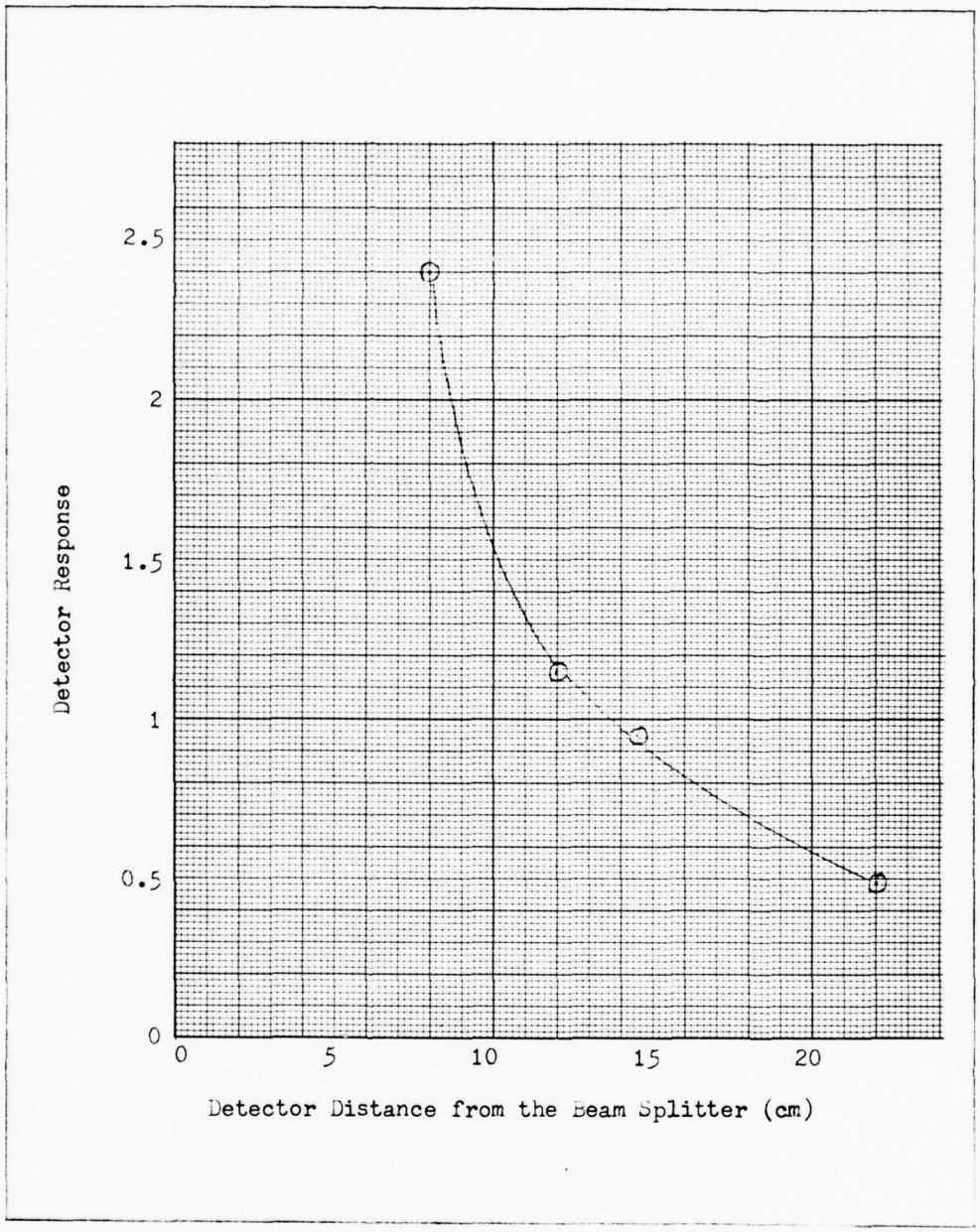

Figure 14. Background Signal at $i + r = 0$ as a Function of Distance from the Detector to the Beam Splitter

beam splitter at a distance of about 3 m each from the beam splitter. The lampblack surfaces gave a very small radiation return to the measurement system. The detector response as a function of detector to beam splitter distance is shown. Scatter from the beam splitter obviously presented a significant background signal to the measurement of the radiation reflected from the nonspecular surface, as in Figure 11. At one time, the chopper was positioned between the beam splitter and the reflecting surface to suppress this background from the real data. This made all data relative to the reflected signal from the chopper. Scanning off-axis presented a parallax problem with the reference spot on the chopper, so this technique was abandoned.

All the measurements accomplished in this experiment were with a beam splitter to detector distance of 8 cm, and the beam split at the beam splitter out into the room was always incident on a chalkboard on the laboratory wall.

The background for each measurement series for a given nonspecular surface was always recorded. The background was measured by removing the nonspecular reflecting surface which allowed the incident beam to travel an additional 3 m before encountering a lampblack surface. There was no measurable radiation return from this lampblack surface at the maximum measurement system amplifier gain used. Then, a measurement scan of $0 \leq |i+r| \leq \pi/2$ was

repeated as accomplished with a sample reflecting surface in position.

The background radiation level for a given incidence beam diameter was constant at a constant i+r , so the measured background linearly varied with the measurement system amplifier gain. An example of the measured background is shown in Figure 15 for the maximum measurement system amplifier gain used for any measurements. The background signal decreased linearly with a decrease in system gain such that it was negligible for measurements of the reflected intensity from highly reflecting surfaces. The large spike at 0° was due to laser beam spot scatter from the beam splitter, and the second small spike at 2.5° was due to the scatter from the edge of the beam splitter. The technique for avoiding the scatter from the edge of the beam splitter, as done here, is described in the experimental procedure.

Detector. The two detector factors which affected the reflected intensity measurements were the field of view of the detector assembly and the detector linearity. The spectral sensitivity of the photomultiplier tube was not a problem due to the narrow emission wavelength band of the laser, and the narrow bandpass filter included in the detector assembly limited any outside band wavelength sources. The position and angular incidence sensitivity of

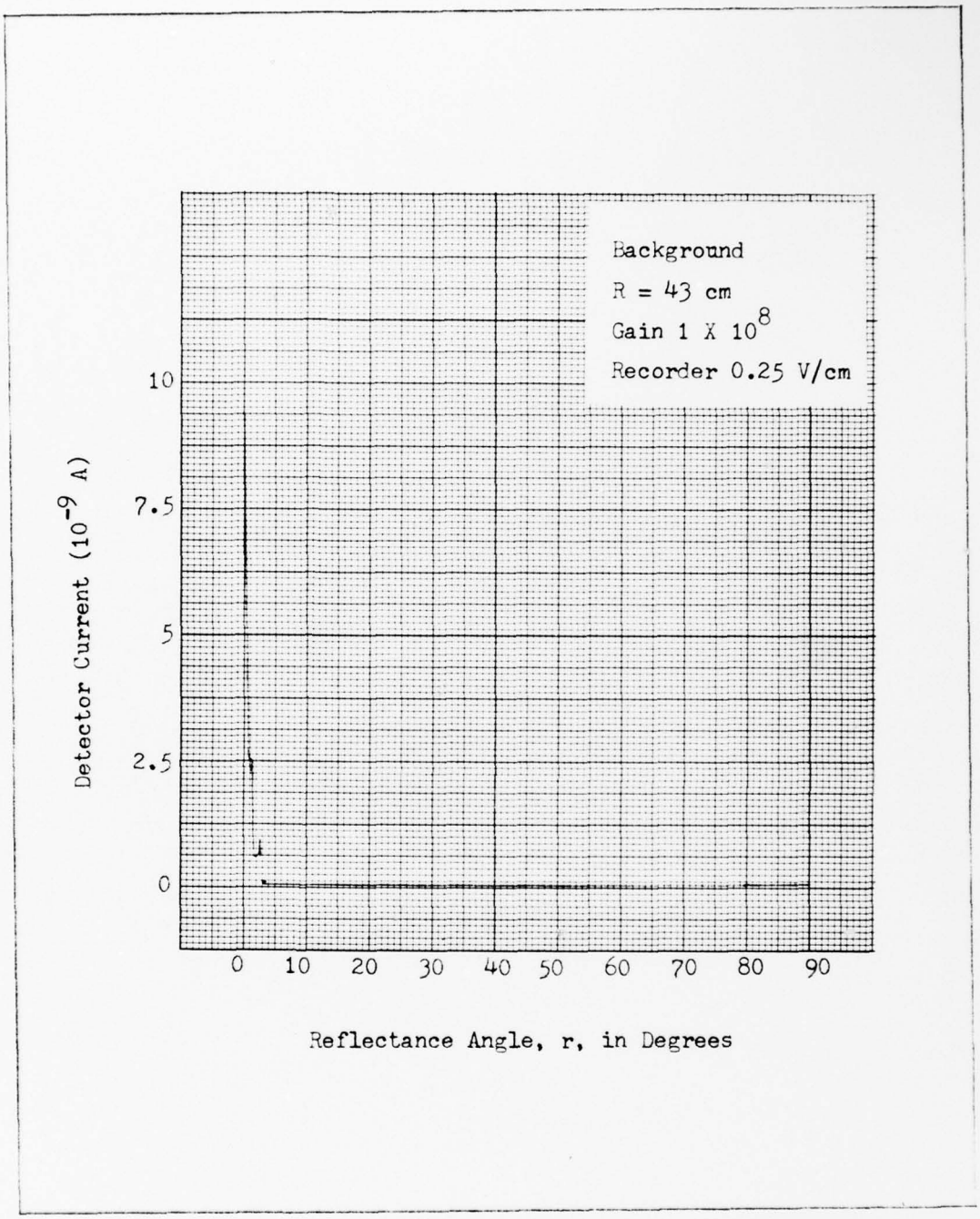

Figure 15. Background Signal at a Maximum System Gain of 10^8 (Axes Are Not Shown to Illustrate the Data)

the first photomultiplier dynode was eliminated by the two small field limiting apertures in front of the photomultiplier tube. A bias supply voltage of 670 V on the photomultiplier tube was used for all measurements.

The detector field of view is shown in Figure 16. With the detector assembly placed directly facing an attenuated beam from the beam expander, the detector assembly was rotated according to the angles shown while the position on first aperture was fixed. The clear field of view of the detector assembly was 1°.

The detector linearity was established by the same set-up as above. With an on-axis detector alignment with an attenuated laser beam, the incident beam was further attenuated using neutral density filters. Below a photomultiplier tube current of 2 μA at an operating voltage of 670 V, the response of the photomultiplier was sufficiently linear that no correction to the measured data is required.

Measurement System Alignment. The final factor which affects the reflected intensity measurements was the overall system alignment. The alignment of the incident beam from the beam expander was addressed earlier. The principal alignment problem was aligning the beam splitter and detector assembly directly on the autoreflectance peak. At a measurement distance (from the nonspecular surface to the detector) of 1 m, the detector aperture subtended only about 0.1°. The

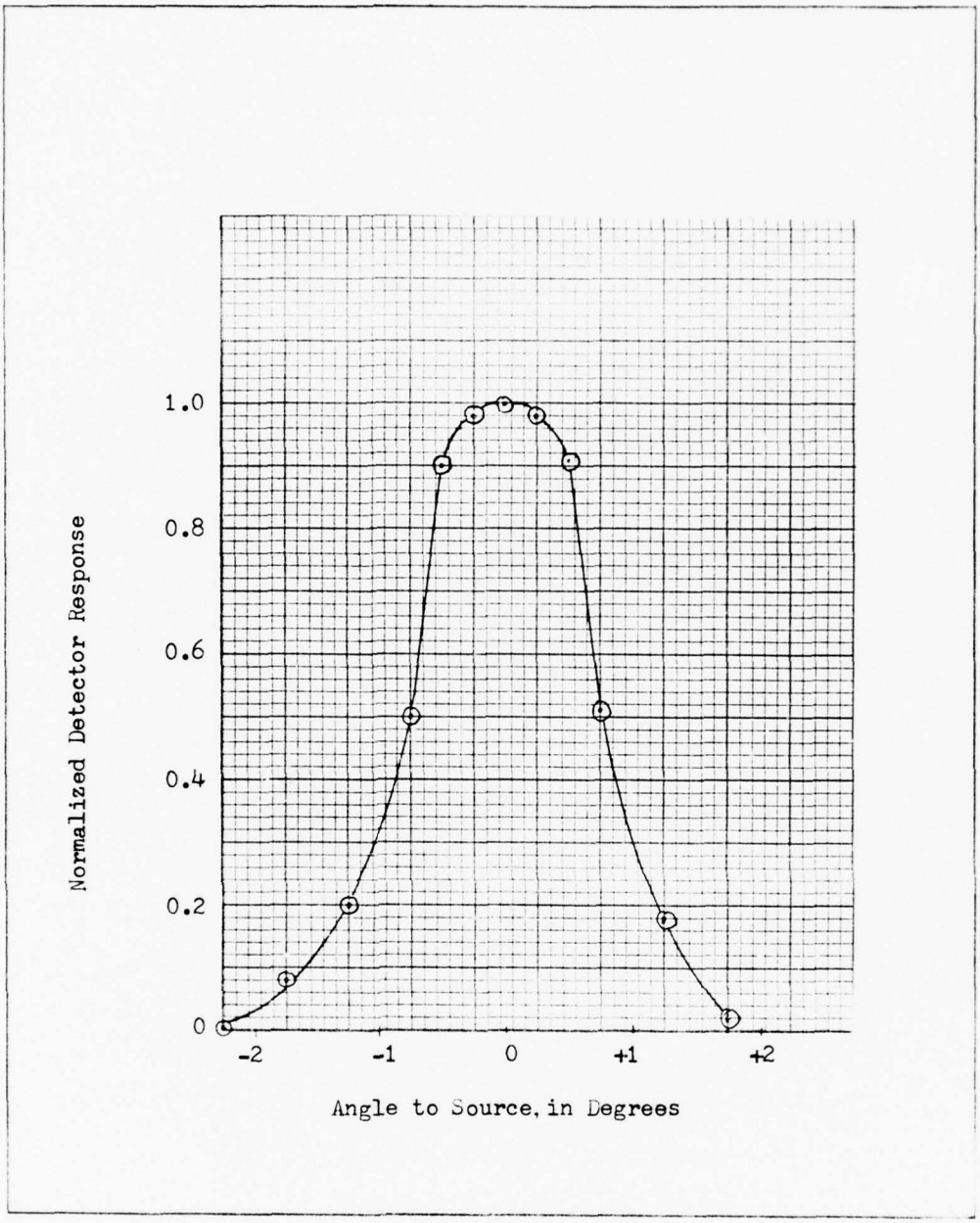

Figure 16. Detector Field of View

radiation was reflected from a circular area of the nonspecular surface which subtended a maximum angle of about 0.2°, so the angular reflected intensity resolution was determined principally by the angular breadth of the spot on the reflecting sample from the detector. These very small angles made the beam splitter and detector alignment critical. These small angles were nevertheless required because the autoreflectance peak was very sharp and varied rapidly with small angle changes near the autoreflection direction.

Experimental Procedure

The individual components of the measurement system were each operated according to manufacturer's operation manuals with the exception of the beam splitter which was fabricated in-house. A minimum warm-up time of one hour for all system components was always allowed before data runs were accomplished. After warm-up, the individual components were aligned along the two measurement system axes for $i+r = 0$ (laser to surface axis and the detector to beam splitter axis). The angle i was appropriately set, and the system amplifier gain adjusted to give a reasonable scale on the Y scale of the X-Y recorder for the particular surface to be measured at the distance of measurement.

Data were recorded by dropping the recorder pen and manually sliding the triangular bench gently about the pivot axis until the edge of the incident beam touched the edge of the beam splitter. At this point, the scan was stopped momentarily, and the recorder pen was lifted. The beam splitter and the detector assembly could be moved transverse to the triangular bench by the transverse adjustment screw on the triangular base mount a distance necessary to move the beam splitter out of the path of the incident beam. Now, the detector was translated this same distance parallel to the triangular bench toward the reflecting surface using the detector translation stage. This maintained the detector field of view alignment with the same spot on the reflecting surface as originally viewed at $i+r = 0$. This procedure is illustrated in Figure 17 where the distances the beam splitter and the detector are moved are greatly exaggerated for clarity. The distances involved were usually about 8 mm (depending on beam diameter). Now the incident beam was not attenuated by the beam splitter, so the system amplifier gain was corrected accordingly. For 0° polarization, the gain was decreased by a factor of two. The recorder pen was dropped, and data were recorded further by slowly swinging the measurement arm out to $|i+r| = \pi/2$. This procedure results in a complete, two segment scan of

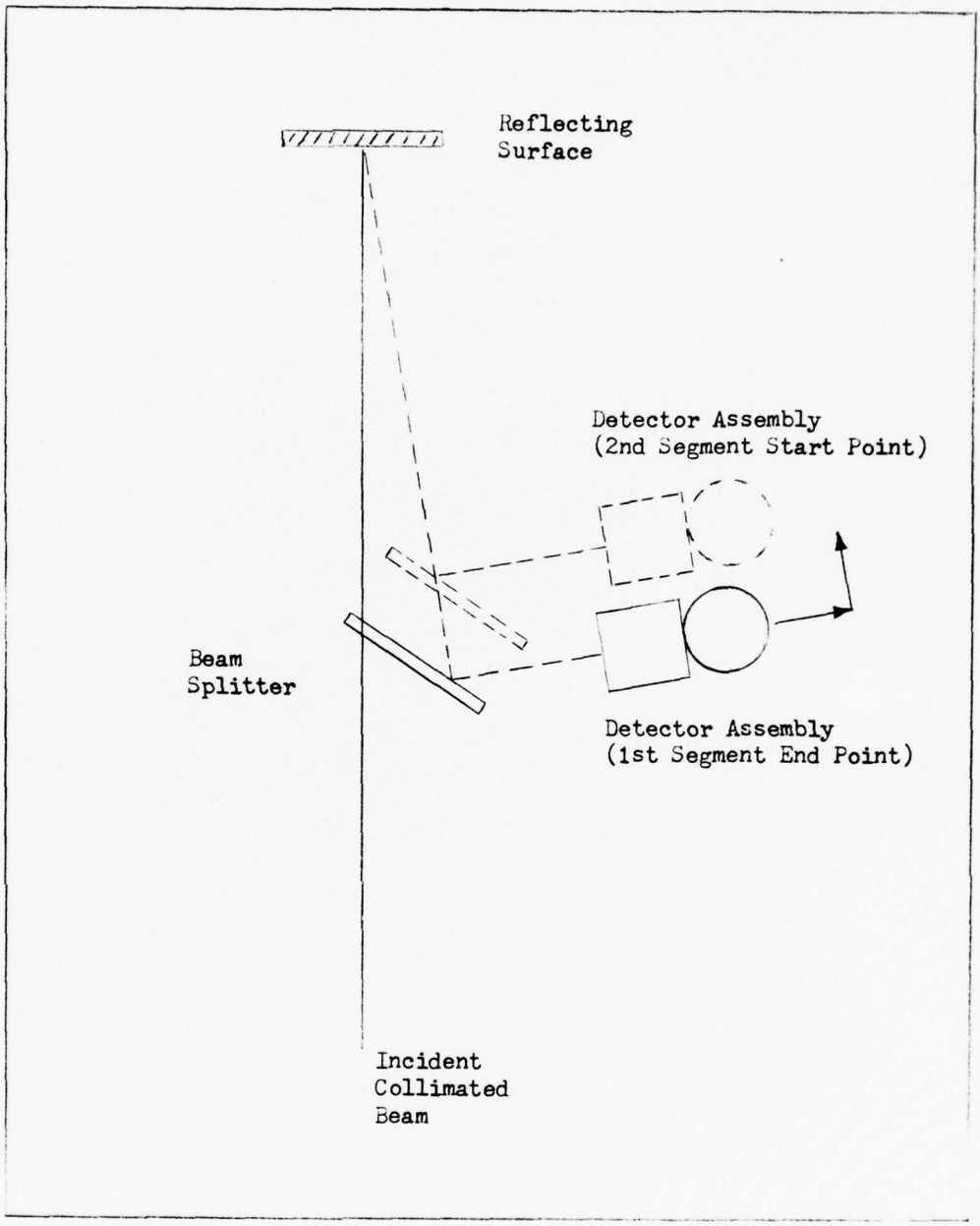

Figure 17. Changeover Procedure for the Two Segment Reflectance Scan (Dimensions Exaggerated)

$0 \leq |i+r| \leq \pi/2$. The total scan time was normally about 2 minutes with about 30 seconds for the segment changeover.

A background scan was accomplished by resetting the measurement arm to $i+r = 0$, the beam splitter and detector positions, and the measurement system gain. The nonspecular reflecting surface was removed which allowed the incident beam to pass an additional distance of about 3 m to a lampblack surface. The measurement procedure of the preceding paragraph was then repeated to accomplish the background scan. The background was removed by subtraction from the reflectance data for the reflecting surface.

IV Experimental Results

The results are presented by first examining the surface microstructure of the five nonspecular surfaces with scanning electron microscope photographs. An example of the reflected radiation interference pattern from the polymeric bead paint surface as measured with a photographic exposure is presented, and the convolution of the interference pattern and the measurement aperture is discussed. The nonspecularity of the reflecting surfaces, the consistency of the reflectance from different areas of the reflecting surfaces, and the consistency of the reflectance data for different measurement distances is demonstrated. Then, the experimental reflectance data for the (1) MgO, (2) $MgCO_3$ block, (3) nonspecular gray paint, (4) polymeric bead paint, and (5) 3M Company Black Velvet paint are presented. Finally, measurements of the dependence of the autoreflectance peak magnitude on measurement distance and the angle of incidence are presented, and the effect of the linear polarization angle of the incident radiation is discussed.

Surface Microstructure

The surface microstructure of each of the nonspecular reflecting surfaces measured is documented by field emission electron microscope photographs. The photographs

were obtained with a Coates and Welter Model 100-2 CWIKSCAN electron microscope. The photographs are images from a cathode ray tube viewing screen. Figures 18-22 are the electron microscope images of the (1) smoked MgO, (2) $MgCO_3$ block, (3) nonspecular gray paint, (4) polymeric bead paint, and (5) 3M Company Black Velvet paint surfaces, respectively. Figure 23 is a blow-up of a portion of the black velvet paint surface to illustrate the microencapsulation of particles in the larger spheres of Figure 22. Each of the surfaces are oriented at 45° to the incident electron beam and the field emission detector, except the MgO surface which is oriented at about 30° to the detector. The direction of surface tilt and the magnification as seen on the photographs are indicated on the individual figures.

In the development of the theory, it was assumed that the model surface was made up of spherical particles which were large with respect to the incident radiation wavelength. Figures 18-21 indicate that only the MgO, polymeric bead paint, and the black velvet paint surfaces are formed by spherical particles. The $MgCO_3$ block surface and the nonspecular gray paint surface are not composed of spherical particles; however, since the autoreflectance peak predicted by geometric shadowing (without considering any glory interference) is relatively insensitive to the shape or size of the particles which form the surface, Eq 20 can

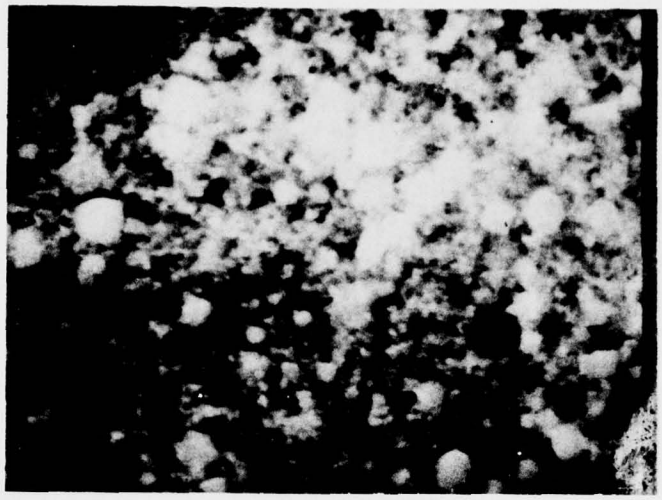

Figure 18. Electron Microscope Image of the MgO Surface (X5000 Magnification)

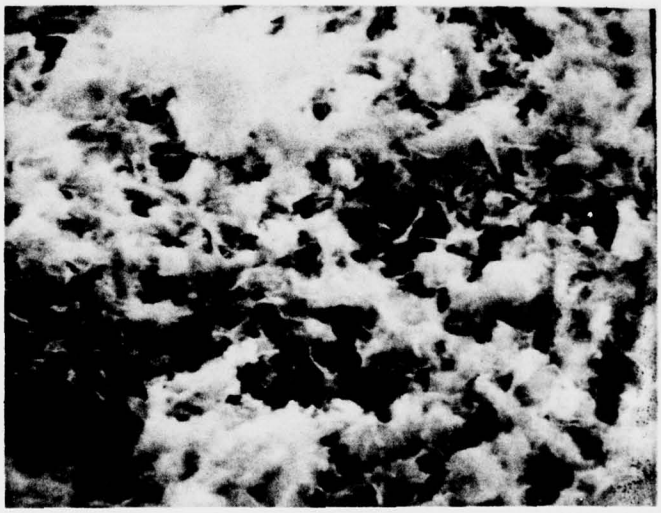

Figure 19. Electron Microscope Image of the $MgCO_3$ Surface (X500 Magnification)

Figure 20. Electron Microscope Image of the Nonspecular Gray Paint Surface (X500 Magnification)

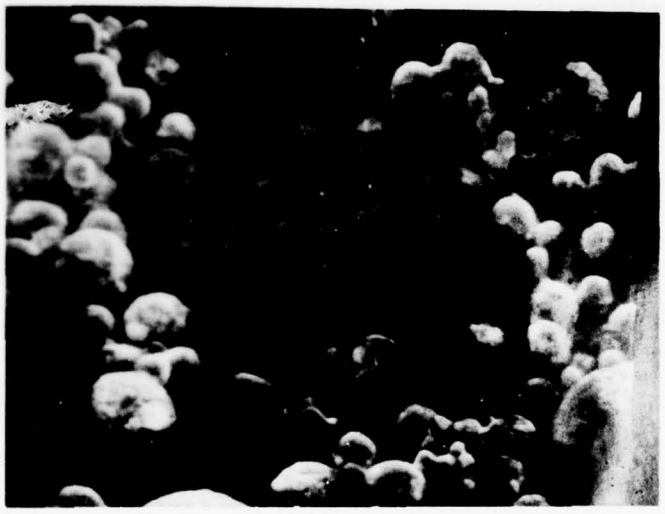

Figure 21. Electron Microscope Image of the Pigmented, Polymeric Bead Paint (X500 Magnification)

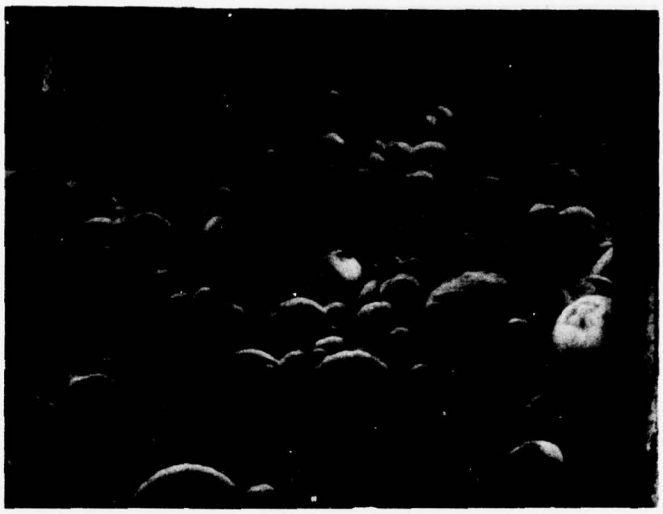

Figure 22. Electron Microscope Image of the 3M Company Black Velvet Paint Surface (X500 Magnification)

Figure 23. Electron Microscope Image of the 3M Company Black Velvet Paint Surface (X5000 Magnification)

still be applied to these surfaces by neglecting the glory term. Also, neither the MgO nor the black paint surface would be expected to exhibit any glory interference because the MgO surface particles are too small and the black paint spheres are too absorbing. The only one of the five surfaces considered which really satisfies the assumptions made in the theoretical development and is relatively transparent to the incident radiation such that the glory term may be significant is the pigmented, polymeric bead paint.

Resolution of the Measurement Aperture

The collimated laser radiation incident on the real surfaces considered is reflected into a very complicated intensity pattern. In the development of the reflected intensity equation, Eq 20, it was stated that the measured reflectance would be in accordance with the interference intensity envelope if the measurement aperture was sufficiently large not to resolve the individual interference peaks. Figure 24 illustrates the complexity of the interference pattern of the radiation reflected from the polymeric bead paint. Figure 24 is a 3 cm diameter, open aperture photograph (no lens) of the interference pattern centered on the autoreflectance peak. The reflecting surface to film plane distance is about 70 cm. It is obvious that a 1.6 mm measurement aperture will not resolve the individual interference peaks, so scanning the measurement

Figure 24. Photograph of the Reflected Radiation Diffraction Pattern About the Autoreflectance Peak

aperture in one dimension will convolute the spatial data into a relatively smooth measured reflected intensity distribution. At the same time, the 1.6 mm measurement aperture is small enough not to artificially broaden the autoreflectance peak.

Nonspecularity of the Reflecting Surfaces

Figure 25 is a sample of a raw data detector response scan for the MgO surface at normal incidence. The background spike at 0° for this measurement system gain is less than 1 mm high so no background removal is required. Figure 26 is a sample scan for the same MgO surface with a 30° incidence angle. The MgO surface is definitely nonspecular, and the autoreflectance peak is obviously still present at $i+r = 0°$. The same check for specularity was used for all the reflecting surfaces studied, and all the surfaces demonstrated the same degree of nonspecularity as the MgO surface.

Uniformity of the Reflecting Surfaces

The repeatability of the reflectance measurements as dependent on the position of the laser spot on the surface is indicated in Figure 27. This figure shows three reflectance scans for three selected areas of the $MgCO_3$ block, two near opposite edges of the 7 cm block surface and one near the center, obtained by translating the surface. This

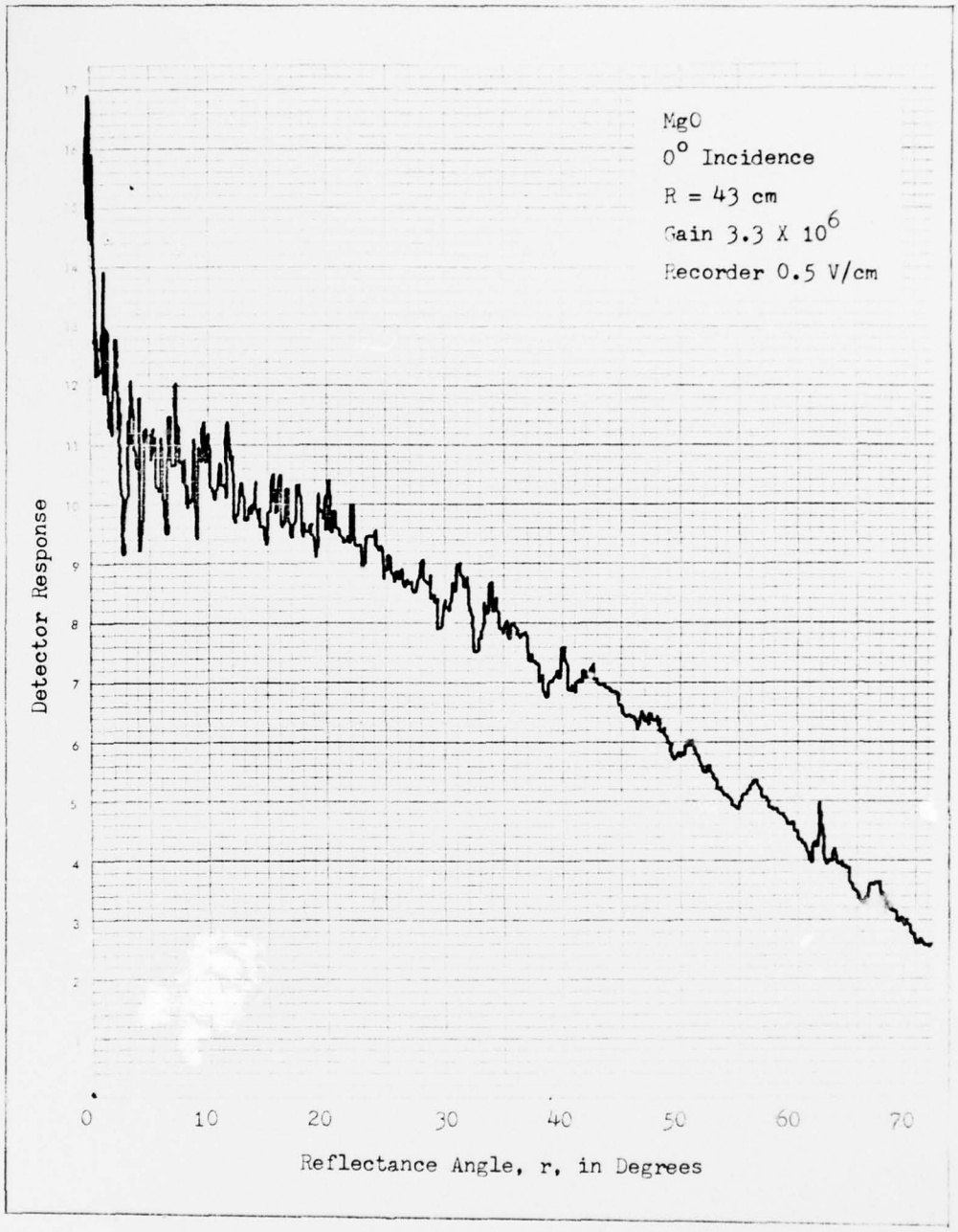

Figure 25. Raw Data Scan for the MgO Surface at Normal Incidence

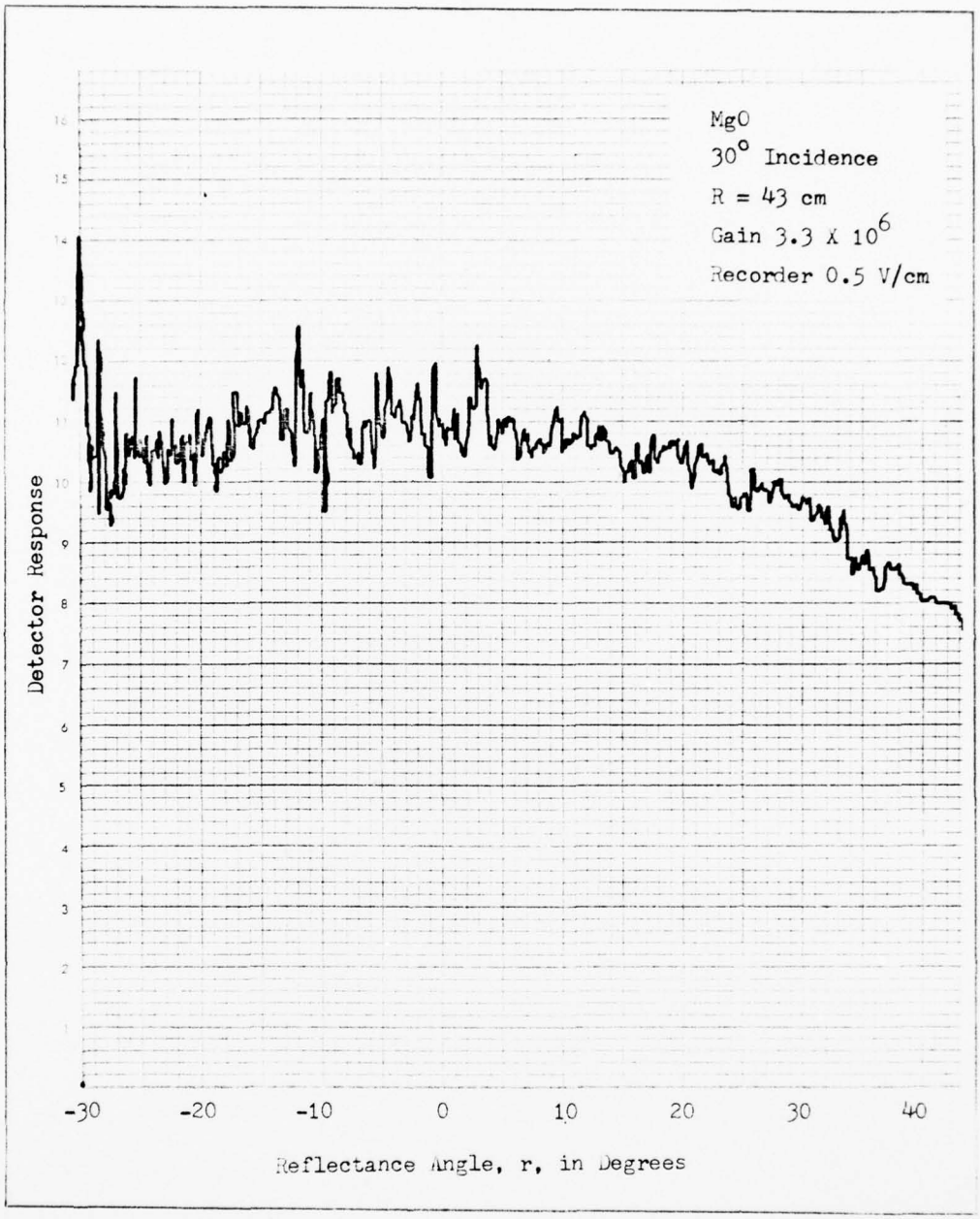

Figure 26. Raw Data Scan for the MgO Surface at 30° Incidence

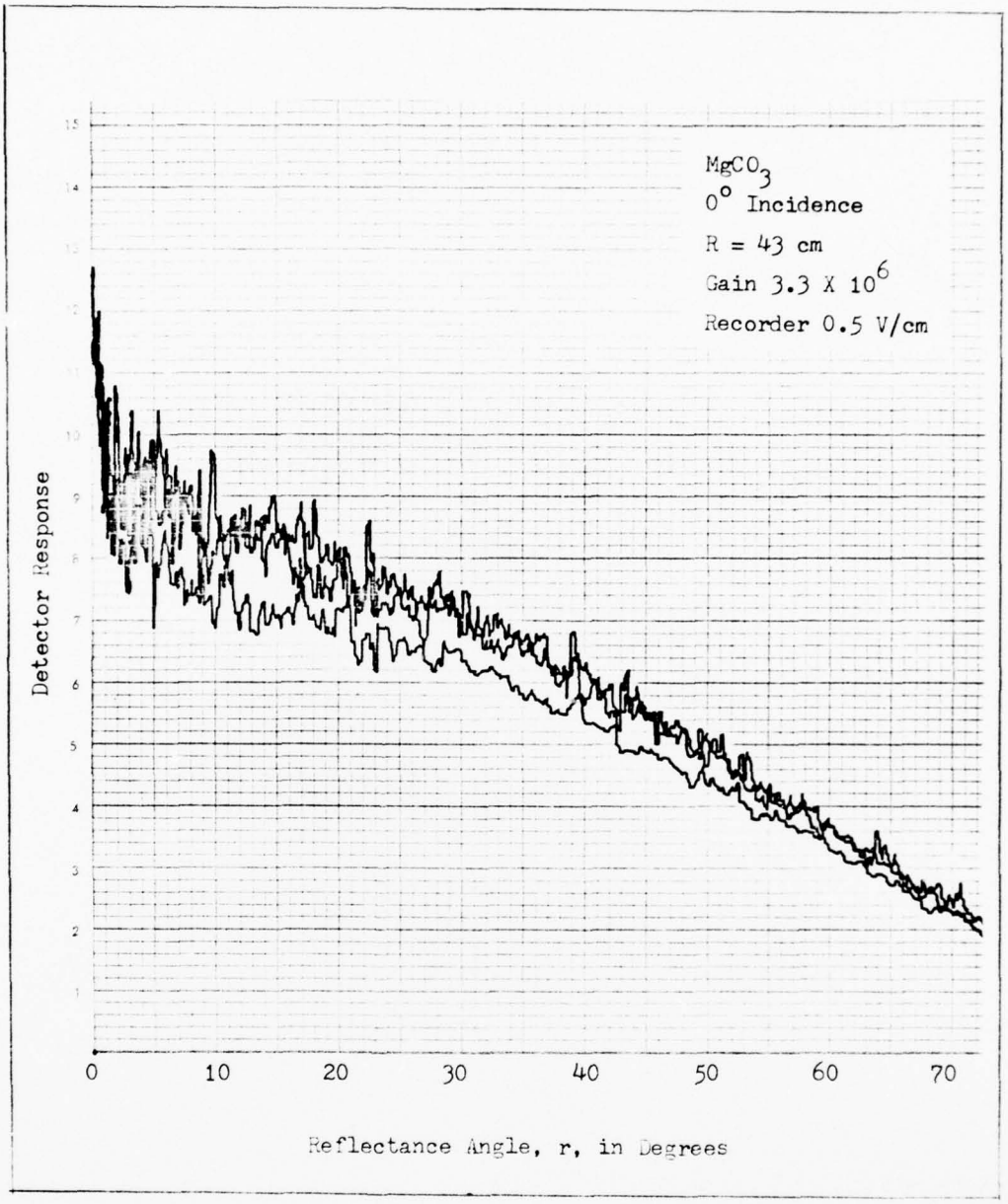

Figure 27. Raw Data Scans for the $MgCO_3$ Surface with Normal Incidence at Three Different Surface Positions

variation in the reflectance as a function of the position of the beam spot on the surface is the worst case found for any of the five surfaces.

Consistency of the Reflectance Data

The small spikes in the reflectance data curves are partly resolved interference peaks. This is illustrated in Figure 28 where three scans are shown for the MgO surface with normal incidence at three different measurement distances. The laser spot on the MgO surface is held at a fixed position. The consistency of the reflectance variation with the angle (i + r) is apparent. There are some differences in the three scans which are readily explained by two factors. First, the angular resolution of the measurement aperture depends upon the distance to the reflecting surface. A large measurement distance results in greater resolution of the interference peaks. Second, the alignment sensitivity can cause some variation in the reflectance scans, particularly in the small angle region about the autoreflectance peak. The repeatability of the reflectance data was generally very good for each of the surfaces measured.

Experimental Reflectance Data

All the reflectance data for each of the surfaces measured was accomplished according to the procedure

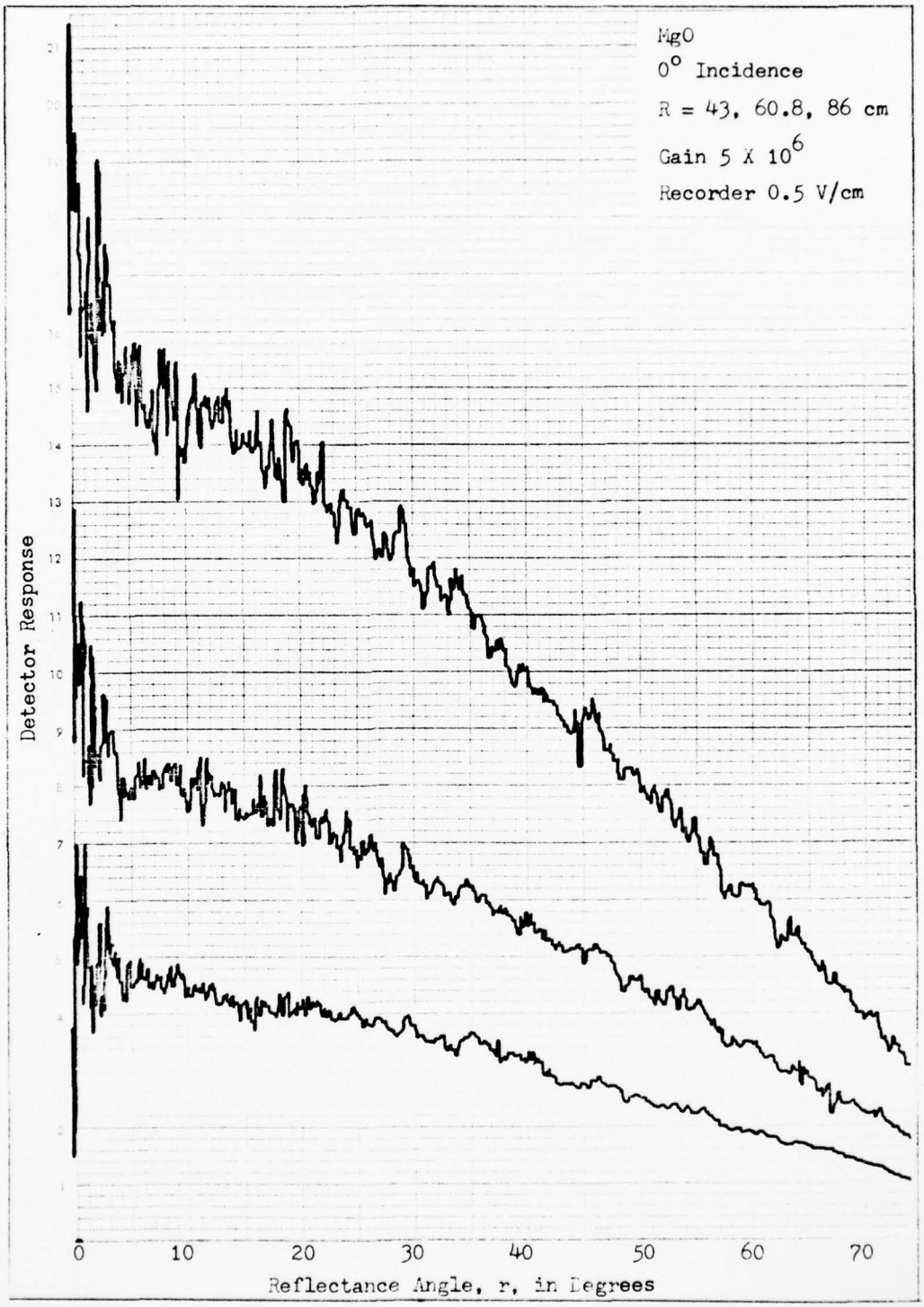

Figure 28 . Raw Data Scans for the MgO Surface with Normal Incidence at Three Different Measurement Distances

described in the experimental discussion. Figures 29-33 are the reflectance distributions for each of the five nonspecular surfaces at normal incidence. The reflectance data is normalized to a theoretical Lambertian reflectance numerically fitted to the detector response curve for the MgO surface with normally incident radiation. The background has been removed, and the curves are smoothed. Each of the surfaces studied exhibits an autoreflectance peak. The black velvet paint surface has a very low reflectance, so the background signal was large as illustrated earlier in Figure 15. This results in some uncertainty in the real magnitude of the autoreflectance peak for this surface, but removing the background signal as described in the experimental procedure results in the data shown. Each of the reflectance curves in Figures 29-33 were accomplished at a measurement distance of 86 cm with the 25.4 mm focal length collimating lens. The laser spot diameter on the reflecting surface with this condition was about 4 mm.

Measurement Distance Dependence

The dependence of the measured magnitude of the autoreflectance peak on the measurement distance was obtained by aligning the beam splitter and detector assembly for $i + r = 0$ and sliding the whole assembly along the triangular base pivot arm. The detector response as a function of measurement distance from the $MgCO_3$ surface with

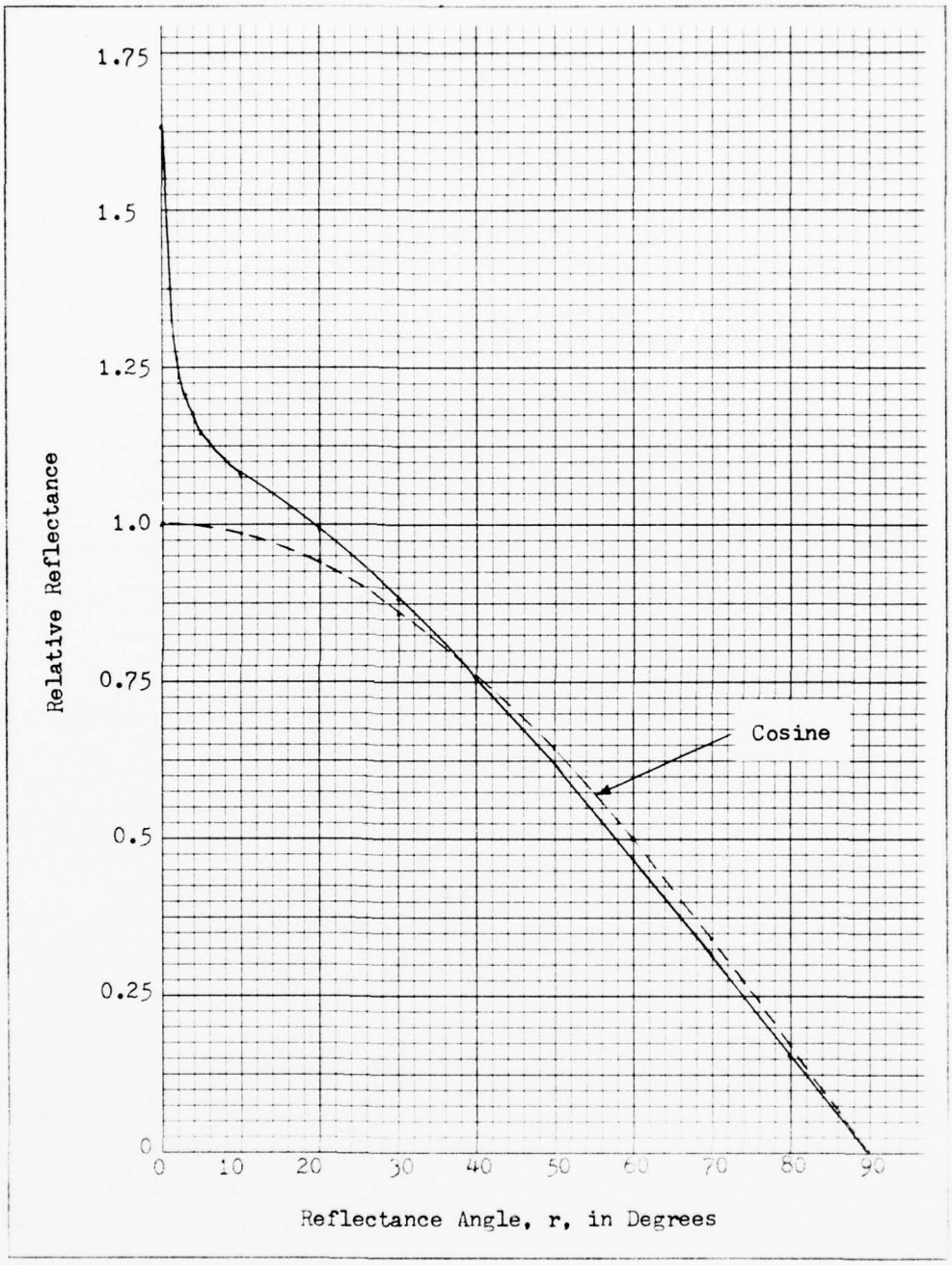

Figure 29. Smoothed Reflectance of the MgO Surface with Normal Incidence

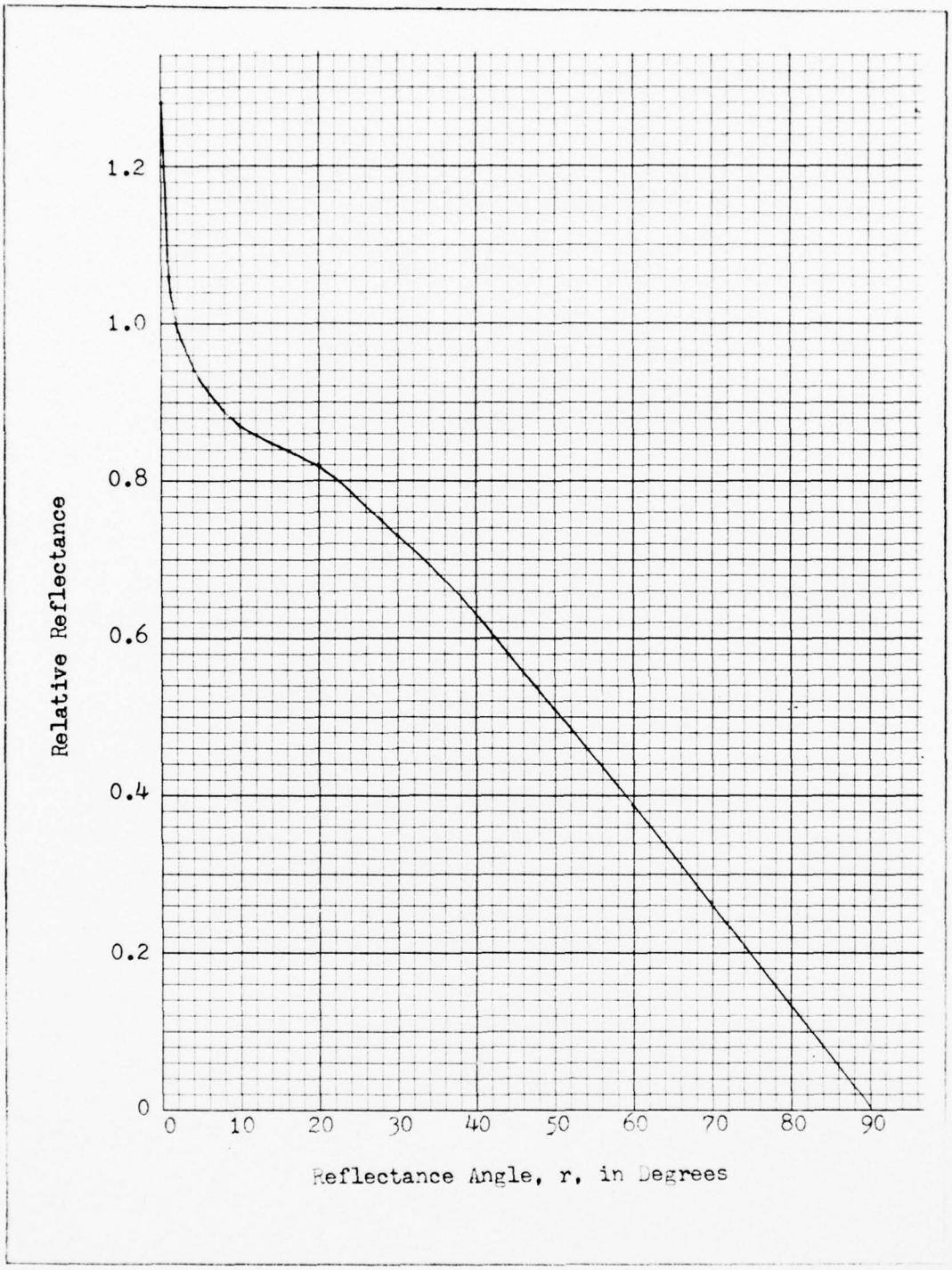

Figure 30. Smoothed Reflectance of the $MgCO_3$ Surface with Normal Incidence

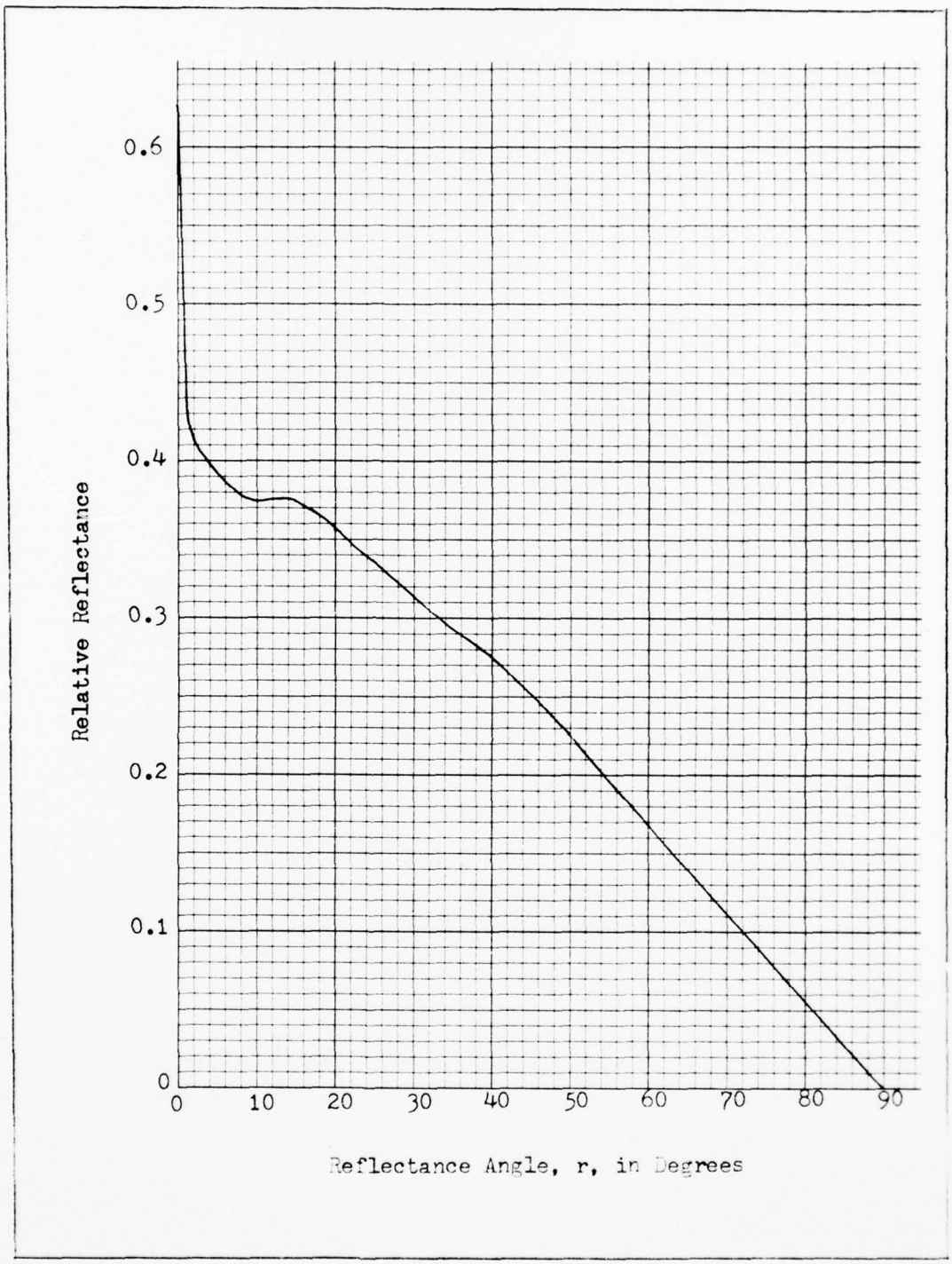

Figure 31. Smoothed Reflectance of the Nonspecular Gray Paint Surface with Normal Incidence

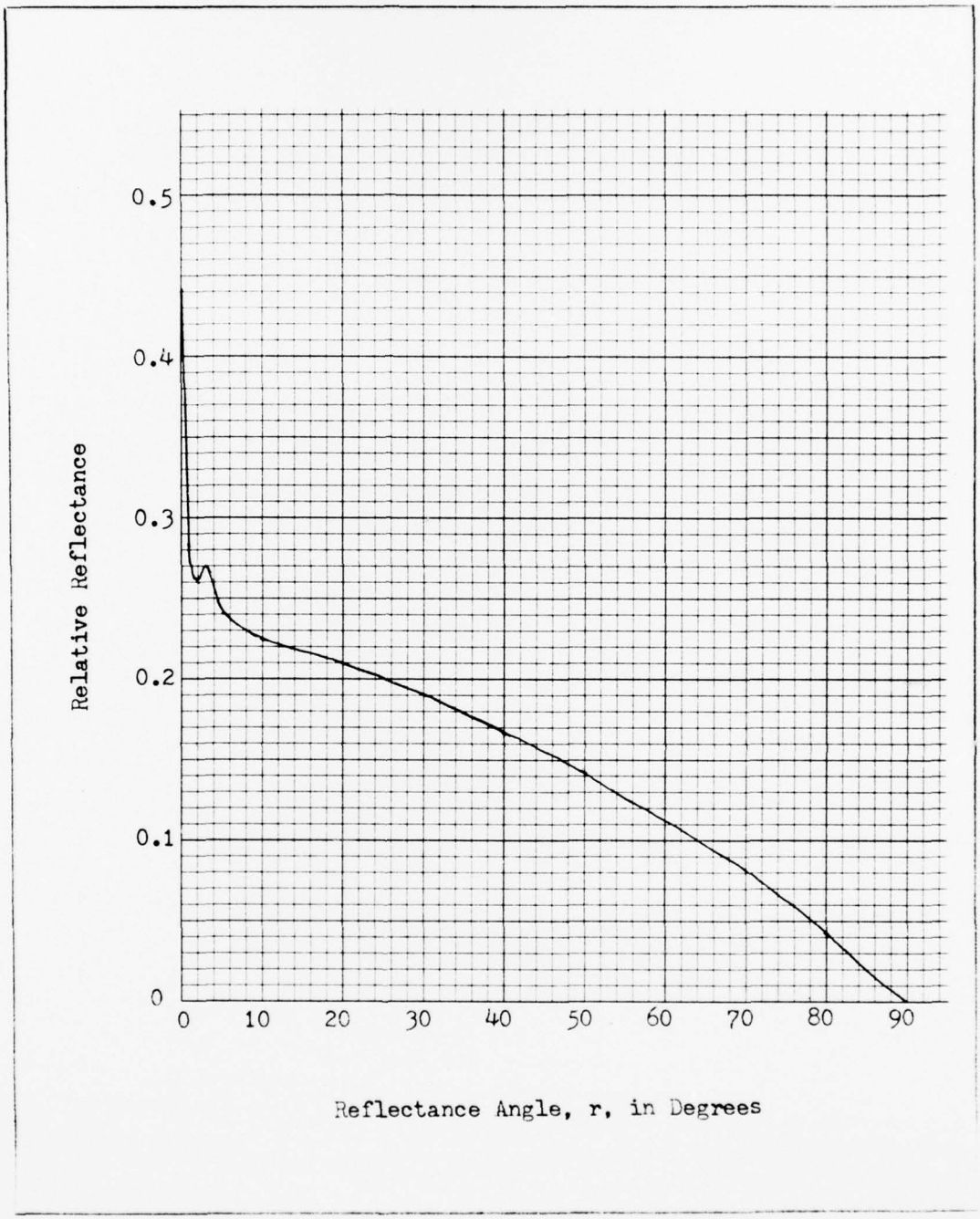

Figure 32. Smoothed Reflectance of the Pigmented, Polymeric Bead Paint Surface with Normal Incidence

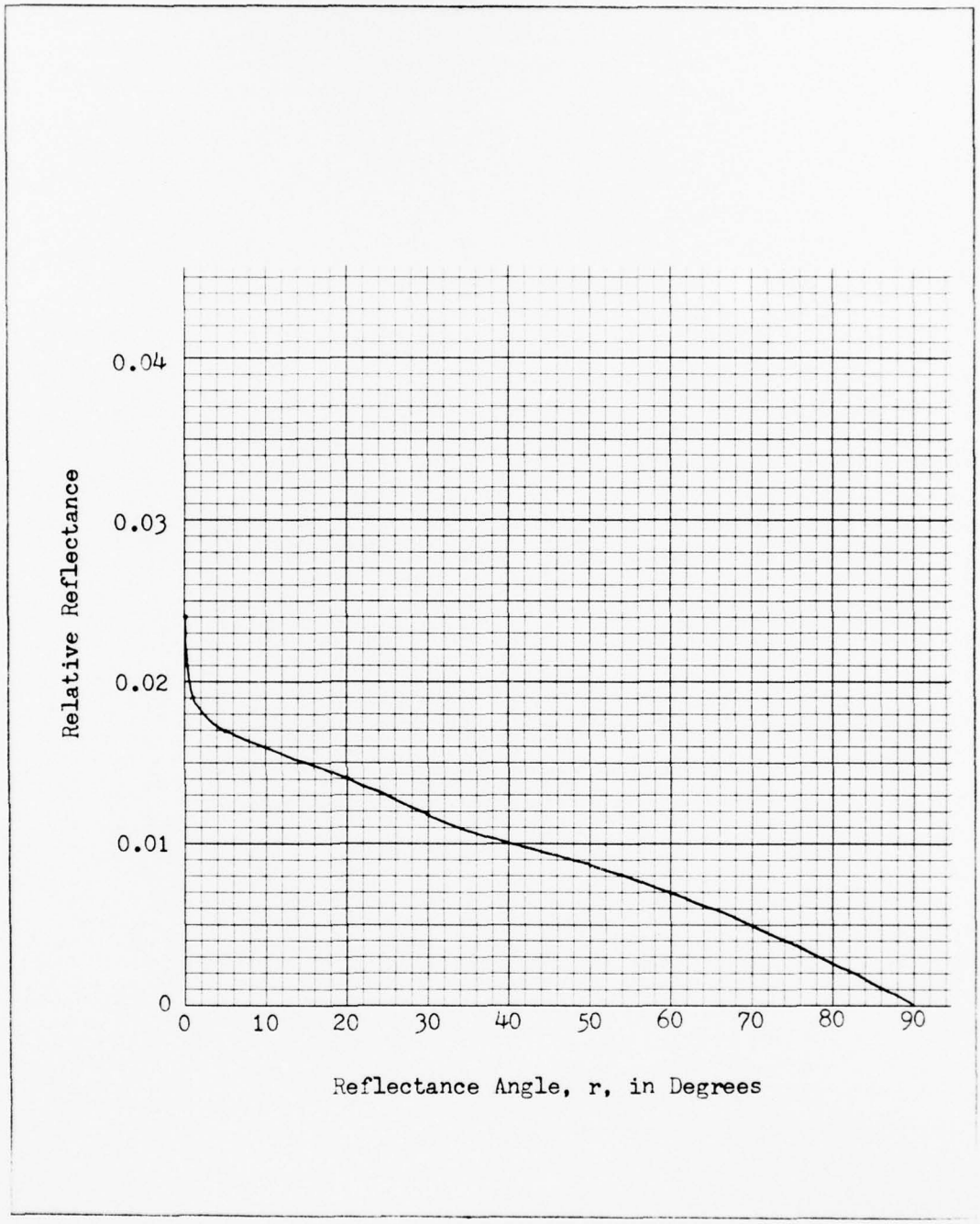

Figure 33. Smoothed Reflectance of the 3M Company Black Velvet Paint Surface with Normal Incidence

normal incidence is shown in Figure 34. The predictions of Eq 20 for this dependence will be examined in the discussion of the results.

Autoreflectance Peak Dependence on Incidence Angle

Another interesting measurement which can be directly performed with the apparatus described in the experiment is the magnitude of the autoreflectance peak dependence on the angle of incidence. The detector and beam positions were fixed such that the detector was always measuring the radiation reflected at $i + r = 0$. The reflecting surface was rotated about the pivot arm rotation axis to achieve a reflectance scan as shown for the $MgCO_3$ surface in Figure 35. The curve does not go to zero at 90° because the incident beam strikes an adjacent face of the $MgCO_3$ block at incidence angles near 90°. The angle of incidence dependence expected from the theory will be presented in the discussion.

Polarization of the Reflected Radiation

To measure the polarization of the reflected radiation, a Glan-Thompson polarizer was introduced between the beam splitter and the detector. Rotation of the half-wave plate at the laser or rotation of the Glan-Thompson polarizer showed that the reflected radiation from the nonspecular surfaces had no preferred linear polarization components

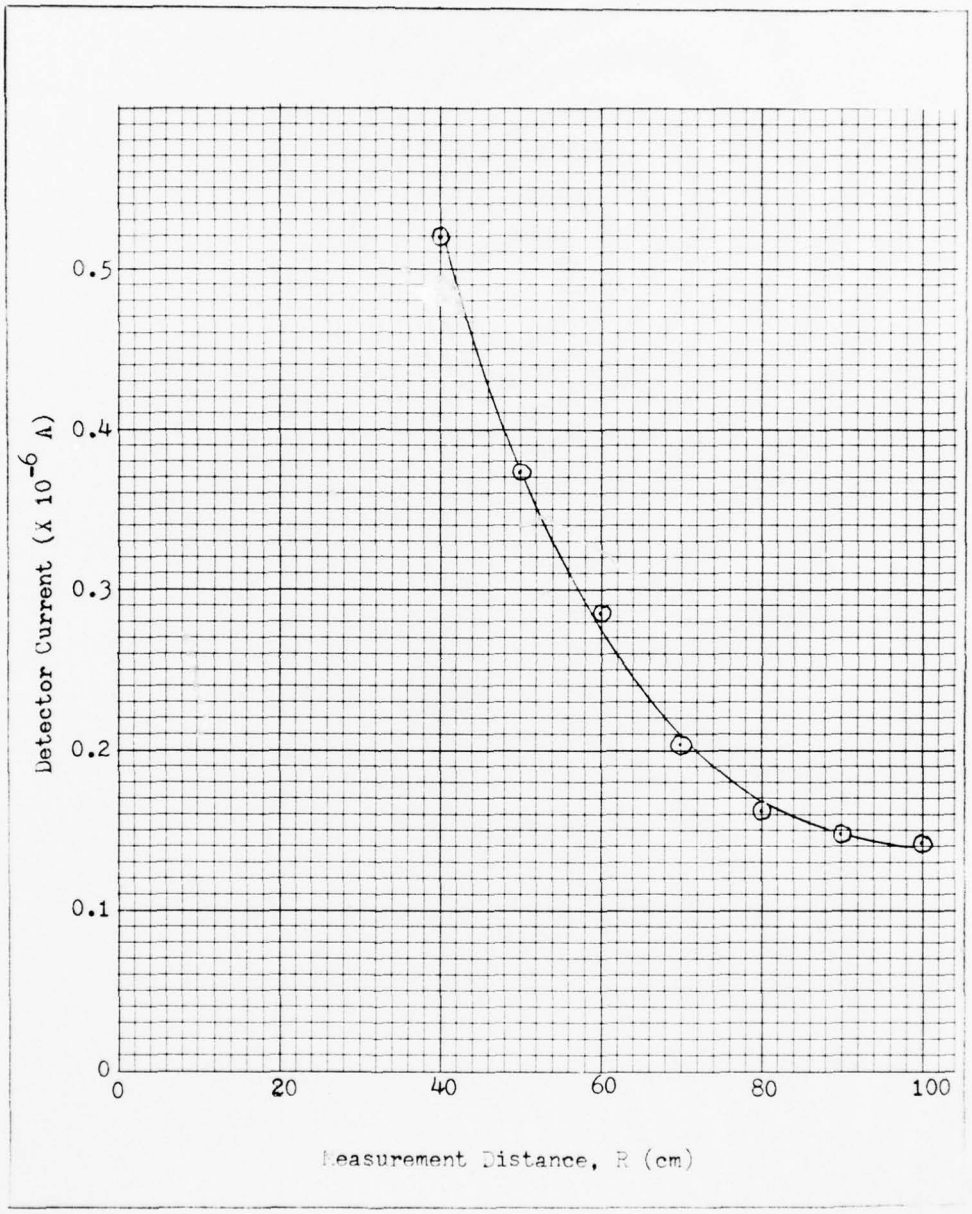

Figure 34. $1/R^2$ Dependence of the Autoreflectance Peak

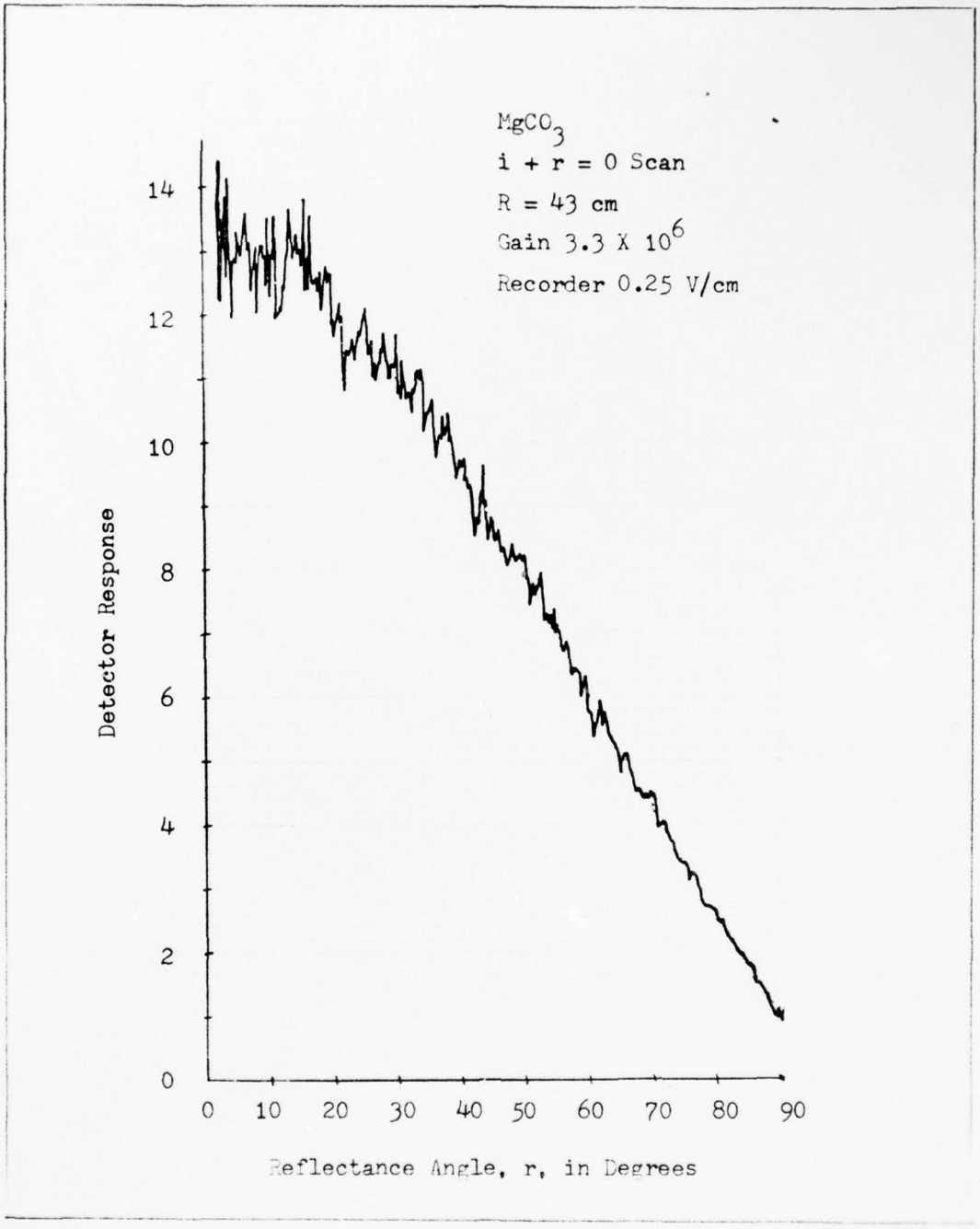

Figure 35. Autoreflectance Peak Dependence on Angle of Incidence

AD-A048 362 AIR FORCE INST OF TECH WRIGHT-PATTERSON AFB OHIO SCH--ETC F/G 20/6
LASER AUTOREFLECTANCE.(U)
DEC 77 C W MARTIN

UNCLASSIFIED AFIT/GEP/PH/77D-7 NL

2 OF 2
AD
A048 362

END
DATE FILMED
2-78
DDC

when the polarizing effects of the system components, as in Figures 12 and 13, are taken into account. To insure that no circular polarization existed, a quarter-wave plate was also placed between the beam splitter and the detector in front of the Glan-Thompson polarizer. The radiation reflected from each of the nonspecular surfaces was completely unpolarized, even in the autoreflectance region with normal incidence.

V Discussion

The experimental results are compared to the reflected intensity equation developed in the theoretical discussion. Eq 20 is applied for the $MgCO_3$ surface to examine the dependence of the autoreflectance peak magnitude on the measurement distance and the angle of incidence. Then, Eq 20 is applied for the pigmented, polymeric bead paint surface and compared to the measured reflectance data for this surface.

Measurement Distance Dependence

The electron microscope image photograph for the $MgCO_3$ surface, Figure 19, showed that the surface was not composed of spherical particles; however, it was argued that the geometric shadowing portion of Eq 20 could still be applied to the reflectance from such a surface because the geometric shadowing is relatively insensitive to the shape of the surface particles. The surface reflecting the laser radiation determines the variables g and b in Eq 7 (which is the same as Eq 20 when glory interference is neglected). If the angles i and r and the size of the measurement aperture are fixed, the measured radiation incident on the detector will be proportional to the square of the distance from the reflecting surface. Figure 36 is

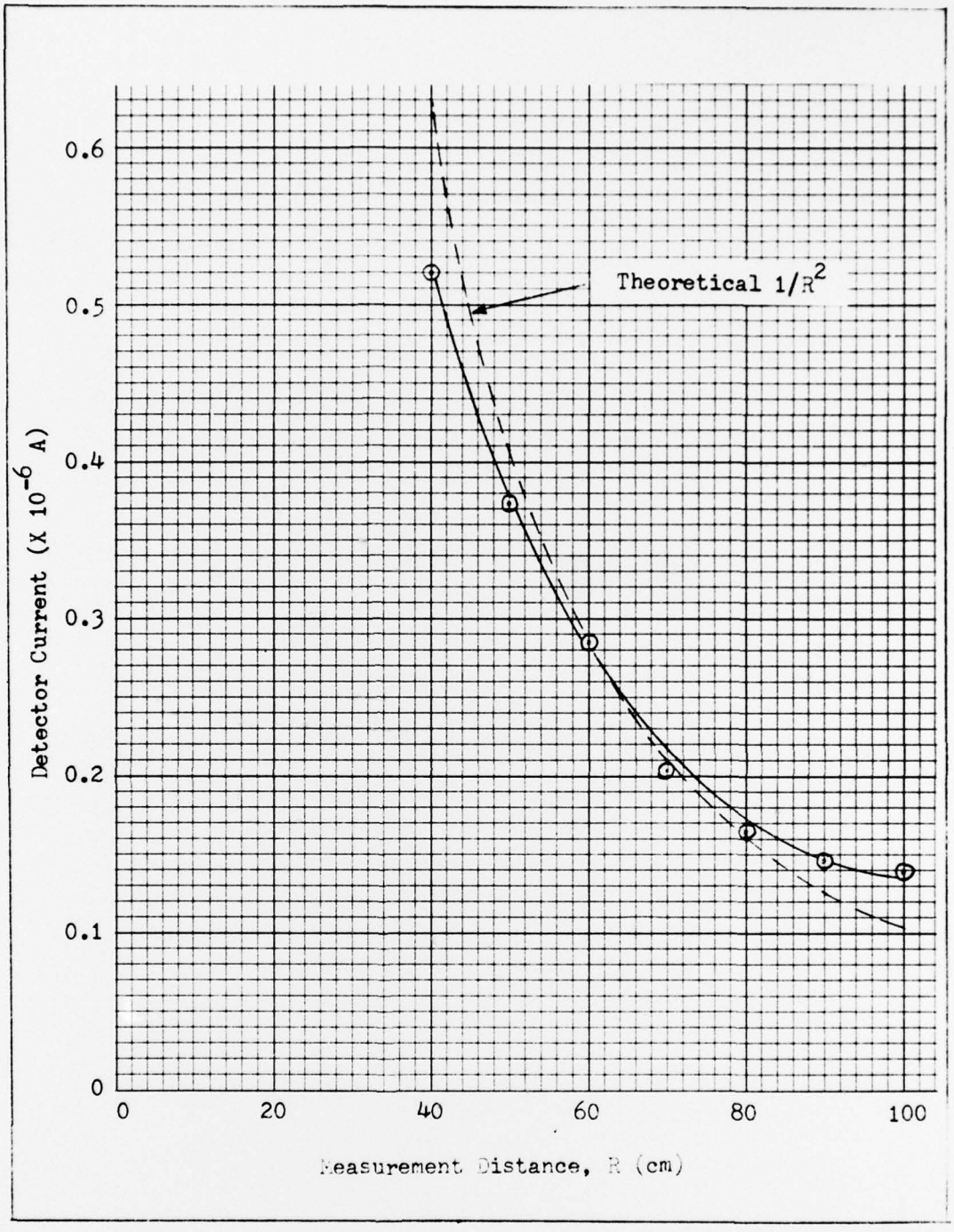

Figure 36. $1/R^2$ Dependence of the Autoreflectance Peak

a comparison of the measured distance dependence of the autoreflectance peak to a fitted $1/R^2$ curve. The fitting was accomplished by intersecting the two curves near the midpoint of each of the curves. The agreement is very good, but the measured data does not exactly fit the theoretical curve. This is to be expected for two reasons. At the smaller distances, the laser spot on the reflecting surface overfills the field of view of the detector, so the measured data falls below the theoretical curve. At the larger distances, the small measurement aperture begins to resolve the individual interference peaks. The measurement system is aligned by "peaking" the detector signal on the autoreflectance peak. This can cause the measured data to be greater than that predicted by the $1/R^2$ curve because the aperture is aligned on a partly resolved interference peak. Once an individual interference peak filled the detector aperture, if R was increased still further, the measured data would be expected to again fall as $1/R^2$.

Angle of Incidence Dependence

When $i + r = 0$, Eq 7 reduces to

$$I = I_o b \cos|r| \tag{21}$$

Thus, when b is constant, the magnitude of the autoreflectance peak goes as $\cos|r|$. This result is compared to Figure 35 for the $MgCO_3$ surface in Figure 37. The

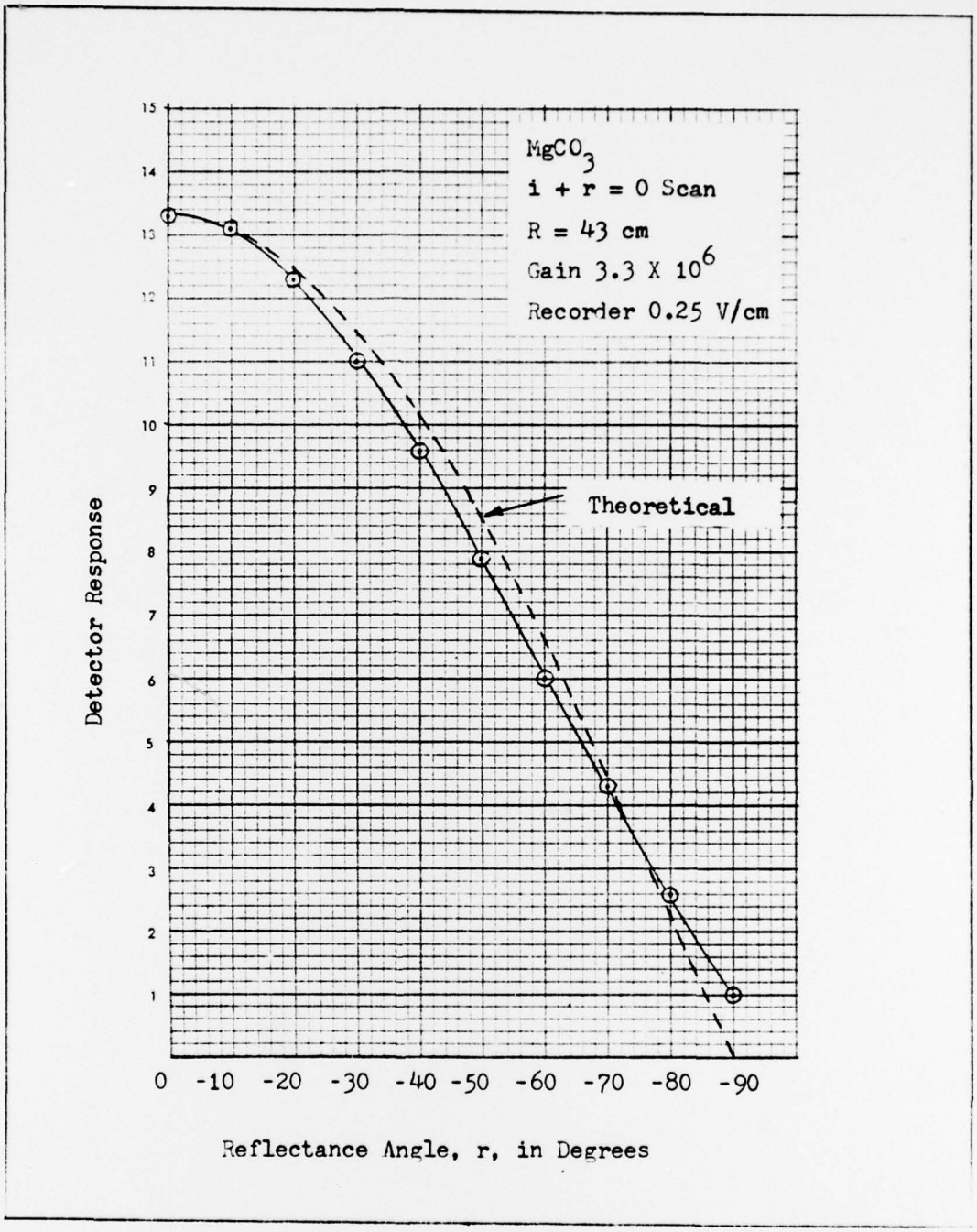

Figure 37. Theoretical and Measured Variation of the Autoreflectance Peak with Angle of Incidence

theoretical curve is fitted at the maximum of the experimental data at 0°. The agreement is excellent except at near $r = -90°$ where the experimental data does not go to zero because the incident beam strikes an adjacent face of the $MgCO_3$ block.

Reflectance Model for the Polymeric Bead Paint

It was stated in the experimental results that of the five surfaces studied, only the polymeric bead paint surface satisfied all the assumptions of the theoretical model surface. The final step in the discussion of the theory and the experimental results is a comparison of the reflectance data for the polymeric bead paint surface and Eq 20 applied for this surface.

In order to apply Eq 20 for the polymeric bead paint surface, g and a can be approximated directly from the electron microscope photograph of the surface, Figure 21. This determination yields a compaction parameter of $g \simeq 0.1$, and an average size particle radius of $a \simeq 5\ \mu m$. The reflectivity coefficient, b, and the glory coefficient, B^2, are most easily determined by fitting to the data of Figure 32. This was accomplished by a trial and error process, and the values selected were $b = 0.22$ and $B^2 = 0.05b$. Eq 20 reduces to

$$I = I \cos r \left[\frac{\sin r + (\pi - r)\cos r}{\pi}\right]$$

$$\left\{\frac{(0.22)H}{1 + \cos r} + (0.01)\left|J_o(49r)\right|^2\right\} \qquad (22)$$

where

$$H = 2 - \frac{\tan r}{0.1}\left[1 - e^{-0.1/\tan r}\right]\left[3 - e^{-0.1/\tan r}\right] \qquad (23)$$

r is used in radians, and $0 \leq r \leq \pi/2$. The result is shown in Figure 38 as the dashed curve, and the solid line is the raw data scan for the polymeric bead surface at normal incidence. A scale is given to indicate the magnitude of the reflectance relative to the MgO surface reflectance normalized to an ideal Lambertian reflector. The background scan is shown at the bottom of the figure. The background has not been removed to show the actual data.

The raw data scan shows that the interference maxima are almost resolved at the distance of 86 cm. The interference effects in the theory were only briefly considered, and then it was argued that the interference effects degraded to the noninterfering intensity envelope with assumptions of a broad particle size distribution and a random particle arrangement. The actual polymeric bead surface does not have an infinite size distribution so the smoothing of the interference peaks is somewhat artificial.

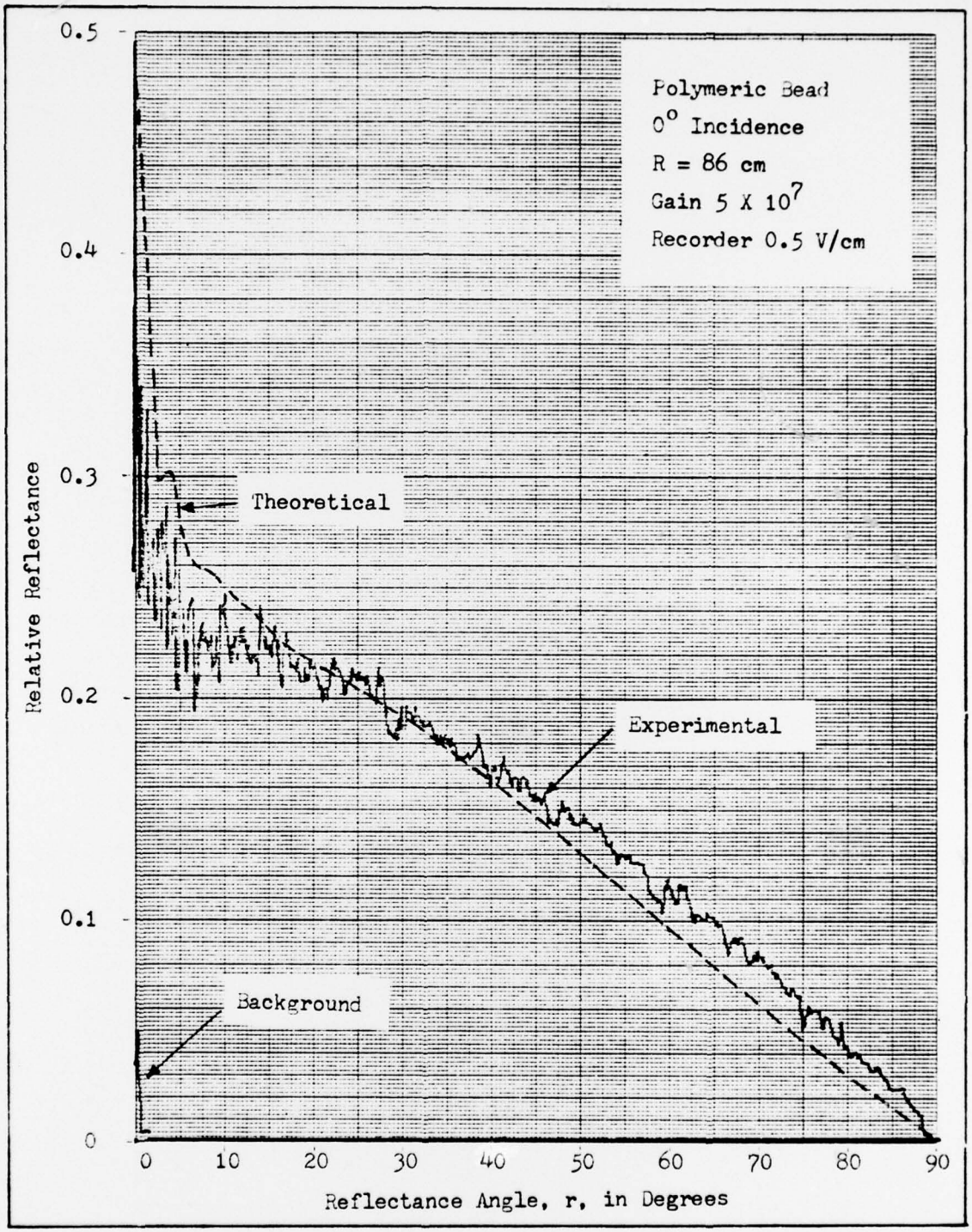

Fig 38. Theoretical and Measured Reflectance for the Pigmented, Polymeric Bead Paint Surface with Normal Incidence

The overall agreement of the theoretical intensity envelope predicted by Eq 22 and the experimental reflectance data for the polymeric bead paint surface is excellent. Particularly note that the second maximum of the glory term occurs at a reflectance angle between three and four degrees for this surface. This portion of the theoretical envelope corresponds very well to the angle position of the average of the experimental data in this region. The theoretical model only considers two terms which arise from geometrical shadowing in the reflecting medium and from glory scatter. The final result of the theory, without resolving the individual interference peaks of the reflected intensity distribution, is a relatively simple equation which predicts the average measured reflected intensity envelope with a surprising accuracy.

VI Conclusion

The object of this thesis effort was to experimentally analyze the reflectance of laser radiation from a small set of nonspecular surfaces and to mathematically model this reflectance. The measurement system and measurement technique described allowed very repeatable measurements to be performed. It was found that each of the five nonspecular surfaces studied exhibited an autoreflectance peak. It was also found that the magnitude of the autoreflectance peak varied inversely with the square of the measurement distance and as the cosine of the angle of incidence on the statistically flat surface studied.

A theoretical surface reflectance model was developed based on Hapke's geometric shadowing theory and van de Hulst's glory theory. It was argued that the interference pattern of the reflected laser radiation from the nonspecular surfaces examined would not be resolved with a sufficiently large measurement aperture such that the measured reflectance distribution would be closely approximated by the geometric shadowing and glory intensity envelopes as developed in the theoretical discussion. Quantitative agreement of this model and the measured reflectance data was shown.

A more elegant theory accounting for interference effects could be developed; however, quantitative validation of such a theory could only be accomplished for a more ideal surface than those studied in this effort. The particle size distribution would need to be extremely narrow, and the particles would need to be arranged in an ordered array. Nevertheless, the reflectance equation developed in this thesis can be applied to most realistic nonspecular surfaces.

The measurements accomplished generally support the previous work of Oetking (Ref 6) and the low coherence length work of Egan (Ref 2). No extremely large (greater than a factor of about two above an ideal Lambertian distribution) autoreflectance peaks were observed when the background was properly removed, so no confirmation of Egan's unusually large autoreflectance peaks (Refs 2 and 3) can be stated. It must be pointed out, however, that the simple reflectance equation developed in the theoretical discussion indicates that very large autoreflectance peaks are possible when the glory scatter becomes more significant than observed with any of the five nonspecular surfaces investigated in this thesis effort.

Bibliography

1. Egan, W. G. Telephone conversation with author on 31 August 1977.

2. Egan, W. G. and T. Hillgeman. "Retroreflectance Measurements of Photometric Standards and Coatings." Applied Optics, 15: 1845-9 (July 1976).

3. -----. "Retroreflectance Measurements of Photometric Standards and Coatings, Part 2." To be published in November 1977 issued of Applied Optics.

4. Hapke, B. W. "A Theoretical Photometric Function for the Lunar Surface." Journal of Geophysical Research, 68: 4571-86 (1 August 1963).

5. Hecht, E. and A. Zajac. Optics. Reading, Massachusetts: Addison-Wesley Publishing Co., 1975.

6. Oetking, P. "Photometric Studies of Diffusely Reflecting Surfaces with Application to the Brightness of the Moon." Journal of Geophysical Research, 71: 2505-13 (15 May 1966).

7. van de Hulst, H. C. Light Scattering by Small Particles. New York: John Wiley and Sons, Inc., 1957.

VITA

Charles Winchester Martin was born 16 April 1946 in Enterprise, Alabama. He graduated from high school in Enterprise, Alabama, in 1964 and attended Enterprise State Junior College and Auburn University. In 1969 he enlisted in the USAF and attended the Special Electronics Technical School at Lowry AFB, Colorado. He served as a reconnaissance system repairman at Shaw AFB, South Carolina, until returning to Auburn University on the Airman's Education and Commissioning Program where he received his Bachelor of Science in Physics. He completed OTS as an honor graduate and subsequently served as a project physicist at the Air Force Armament Laboratory, Eglin AFB, Flordia. He entered the School of Engineering, Air Force Institute of Technology, in June 1976.

Permanent Address: P.O. Box 165
Enterprise, AL 36330